BABAR Analysis Document #418
Version 3.0
July 2, 2003

Report from the Long Term Planning Task Force

The Long Term Planning Task Force has considered the physics impact of increased PEP-II luminosity and possible *BABAR* detector upgrades. Sensitivity projections, with and without detector upgrades, have been examined for a few representative benchmark channels. We find that there is no strong physics case for significant changes to the present detector configuration. However, the physics potential of the experiment will be significantly enhanced by additional improvement to PEP-II luminosity, which will then reach the design limits for the LER vacuum system. Early implementation of a proposed small-angle crossing scheme, perhaps coordinated with the replacement of SVT modules in 2005, could allow the accumulation of data samples in the range from 1–2 ab^{-1} towards the end of the decade. Samples of this size or larger appear to be necessary for measurement of the unitarity *CP* asymmetry angles α and γ.

Direct contributors to this document: Roy Aleksan, Giovanni Batignani, Adrian Bevan, Bob Cahn, Gautier Hamel de Monchenault, Francois LeDiberder, Riccardo Faccini, Francesco Forti, Marcello Giorgi, Yannis Karyotakis, Livio Lanceri, David MacFarlane, Fernando Martinez-Vidal, Tom Mattison, Jim Olsen, Matteo Rama, Blair Ratcliff, Steven Robertson, Mike Roney, Aaron Roodman, John Seeman, Bernhard Spaan, Su Dong, Mike Sullivan, Christos Touramanis, Bill Wisniewski.

Contents

1 Introduction

In March 2002, a *BABAR* task force was formed to examine the impact of possible improvements to PEP-II luminosity and concurrent upgrades to the detector on the physics reach of the experiment beyond 2006. The full charge to the group is provided in Appendex A. It was intended that a strategy be identified for maintaining leadership of *BABAR* in heavy flavor physics in the latter half of the decade, working within the constraints of feasible upgrades to PEP-II, principally to the configuration of the interaction region, and possible improvements to *BABAR*. The charge emphasized the need to minimize down time and therefore loss of integrated luminosity in any upgrade scenario. It was recognized that dramatic improvements in luminosity would require new accelerator and detector facilities, which would represent major new investments by the high-energy community. Such a super B Factory, aiming for luminosities in the range of 10^{36} cm^{-2}s^{-1}, is the subject of ongoing study in the wider community. However, as part of the process of mapping out the future of B physics, this task force was focussed on understanding more precisely the ultimate sensitivity limits of the PEP-II and *BABAR* facility.

The work of the task force has been organized by two groups: Group 1, with emphasis on physics studies, and Group 2, concentrating on exploring detector upgrade options. The common thread to the work of both groups was the identification of a set of representative benchmark processes, described in Section 2, which were used to project physics capability of both the present detector and plausible upgrades to it. Section 3 provides a summary of the discussions within Group 2 of the spectrum of possible upgrades, including moving to an angled crossing scheme for the PEP-II interaction region. Even before our deliberations started, it was clear that the Collaboration would need to address the replacement for the barrel RPC chambers on a fairly short timescale. Therefore, we assumed from the outset that this task would be part of any upgrade plan. Beyond this, the most promising additional detector upgrade possibilities that emerged from our review were (1) a significantly improved vertex resolution through implementation of a small-radius insertion inside the SVT and (2) instrumentation of the B1 magnets close to the IP as an electromagnetic veto counter.

In order to make quantitative physics assessments of the upgrade options, a new fast simulation tool was developed, which allows easy modification to the basic layout of the detector tracking system design. The details of this development are discussed in Section 4, along with validation studies with full GEANT4 Monte Carlo simulation. Section 5 discusses specific scenarios for reconfiguration of the SVT and their implications for vertex resolution. Since there are unquantified risks and technical challenges involved with moving to a smaller radius beam pipe, we chose to look at three different scenarios that span the conceivable range of impact parameter performance.

Based on the matrix of representative physics channels and the identified upgrade scenarios, a number of studies were performed that extrapolate from present physics analyses to make projections of future sensitivity. These studies, reported in Section 6, provide a benchmark for expected performance with data samples corresponding to integrated luminosities of 0.5, 2.0, and 10.0 ab^{-1}. The first of these samples represents the near-term goal of the experiment (2006), the second is a feasible integrated sample for an upgraded version of PEP-II and *BABAR* towards the end of the decade, and the third is a typical

single year of running at a super B Factory. These studies show that improving the impact parameter resolution of *BABAR* does not bring dramatic improvements in physics reach for either time-dependent asymmetry measurements or the determination of V_{ub}. Likewise, the impact of instrumenting the B1 magnets as a veto counter are of marginal benefit to analyses like $B \to \rho\gamma$ or $B^- \to \tau\overline{\nu}_\tau$.

Our conclusions and recommendations based on these studies are presented in Section 7. Balancing the effort and technical risk involved, as well as the additional down time implied, we believe that the present detector, with replacement of the barrel RPCs, is well suited to extended running through the end of the decade, with the possible exception of some specific background problems that need to be further addressed. At the same time, the benefits of an additional factor of two improvement in PEP-II peak luminosity provided by a reconfigured interaction region, if implemented as early as possible, will be a significant benefit to the integrated data sample. Reaching the $2\,\mathrm{ab}^{-1}$ level towards the end of the decade may very well be enough to bring many important physics studies to a much more interesting level of sensitivity, as we continue to search for evidence of new physics in *CP* violating asymmetries and rare B decays.

2 Benchmark channels

Topic	Measurement	Benchmarks
Unitarity triangle constraint	V_{ub}	$B_{\rm rec}$ and $B \to X_u \ell\nu$
	V_{td}	$B \to \rho\gamma / B \to K^*\gamma$ $B \to \tau\nu$ and f_B
	$\sin 2\beta$	$b \to c\overline{c}s$ $B^0 \to D^* D^*$ $B^0 \to \phi K^0_S$
	$\sin 2\alpha$	$B^0 \to \pi^+\pi^-$ $B^0 \to \rho\pi^-$
	$\sin^2\gamma$	$B^+ \to D^0_{CP} K^+$
New Physics	SUSY	$B \to K^{(*)}\ell\ell$ $B \to K^{(*)}\nu\overline{\nu}$
	Lepton no. violation	$\tau \to \mu(e)\gamma$
Tools	Vertexing Tagging	

Table 1: Identified physics goals for benchmark channels.

In order to provide a broad framework for understanding the physics reach of the experiment a number of representative benchmark channels were identified. One goal in selecting this set of channels was to span the range of Standard Model physics and new physics sensitivity. This is illustrated in Table 1. The other goal was to span a range of sensitivities to detector performance and, therefore, detector upgrade possibilities, as

shown in Table 2. The benchmark channels have then been used to project the expected sensitivity of the present *BABAR* detector and various options for detector upgrades.

Benchmark	Vertexing/ Tacking	Angular Coverage	Lepton ID	Hadron ID	K_L^0 ID	Calorimetry
$B_{\rm rec}$ and $B \to X_u \ell\nu$	**	***			***	
$B \to \rho\gamma / B \to K^*\gamma$				***		***
$B \to \tau\nu$ and f_B		***			***	***
sin2β	***	***			***	
sin2α_{eff}	***			***		
$B^+ \to D^0_{CP} K^+$	***			***		
$B \to K^{(*)}\ell\ell$, $K^{(*)}\nu\overline{\nu}$		***	***			
$\tau \to \mu(e)\gamma$			***			

Table 2: Dominant detector system needs for benchmark channels.

3 Luminosity and detector upgrade models

	Design		Achieved	
	e^-	e^+	e^-	e^+
Beam energies [GeV]	9	3.1		
Currents [A]	0.75	2.14	1.05	2.14
Number of bunches	1658		830	
L [$\times 10^{33}$ cm^{-2}s^{-1}]	3.0		4.6	
Bunch spacing [m]	1.26		2.52	
β_x^*, β_y^* [cm]	50/1.5	50/1.5	50/1.25	50/0.9
ξ_x, ξ_y	0.03	0.03	0.070/0.029	0.062/0.056
Bunch currents [mA]	0.45	1.29	1.28	2.20
Beam stored energy [kJ]	49	49	69	41
Beam power [GW]	6.7	6.7	9.4	5.6
Beam rf power [MW]	1.8	1.7	2.5	1.4

Table 3: Original PEP-II design parameters and achieved performance to date.

The record of integrated luminosity so far delivered by PEP-II is shown in Fig. 1. This very successful start for the collider is clearly a remarkable accomplishment. PEP-II reached its design luminosity in the fall of 2000, barely one year after first collisions. Since the fall of 2001 it has routinely been delivering peak luminosity at 50% greater than design and daily integrated rates that are a factor of two over expectations. Some of the main design parameters of the PEP II machine are shown in Table 3, along with the performance records achieved to date.

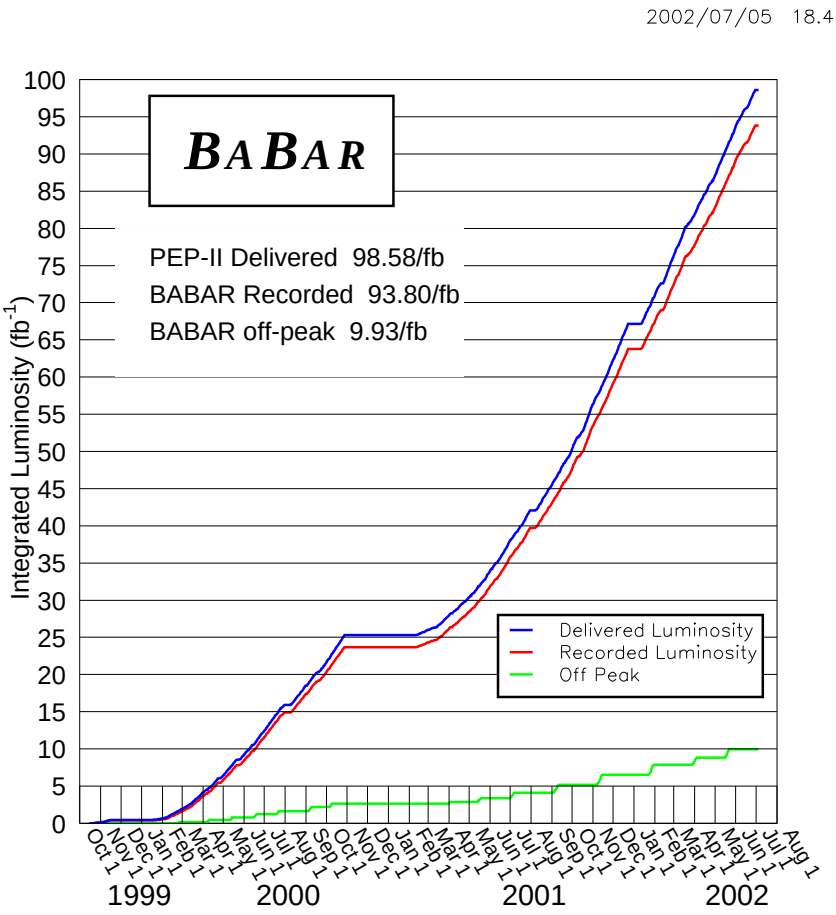

Figure 1: History of integrated luminosity delivered by PEP-II and recorded by *BABAR* through June 30, 2002.

Based on this outstanding record, PEP-II has already embarked on an upgrade plan, which involves the addition 6 more rf stations through the end of 2004. The additional rf will allow shorter bunch lengths, smaller vertical emittance and vertical focusing (β_y^*), and higher beam currents. Step I and II of this plan have already received funding approval by SLAC. Table 4 shows the planned growth of the peak luminosity of the machine, which could reach 2×10^{34} cm^{-2}s^{-1} by the end of 2005. It is on this basis that *BABAR* expects to accumulate 0.5 ab^{-1} of $\Upsilon(4S)$ data by about the end of 2006.

3.1 Crossing-angle scheme for PEP-II

At an asymmetric-energy collider, high-energy (HEB) and low-energy (LEB) beams must be brought into collision at the interaction point and then separated again, without introducing additional parasitic crossings. This is presently accomplished at PEP-II with a head-on collision scheme, where the initial separation kick is achieved with a samarium-cobalt dipole magnet about 20 cm away from the IP. Additional separation is provided by off-axis quadrupole fields. The layout of the interaction region is shown schematically

Parameter	PEP-II Configuration				Units
	Current	Step I	Step II	Step III	
Peak luminosity	5	10	20	40	$\times 10^{33}$ cm^{-2}s^{-1}
I_+	1850	2700	3600	4500	mA
I_-	1050	1400	1760	2000	mA
β_y^*	11.5	9	7	4.5	mm
β_x^*	50	50	50	50	cm
No. of bunches	792	1300	1500	1600	
Vert. emittance	2.5	1.4	1.1	0.7	nm
Horiz. emittance (+/−)	40/50	30/45	32/47	40/48	nm
Crossing angle	0	0	0	$\sim \pm 8$	mrad
Tune shifts (x/y)	7.5/4.5	8.0/5.7	8.2/6.0	8.4/6.3	$\times 100$
No. of rf stations	7	10	13	15	
Date hardware ready	Jan 02	Dec 02	Dec 04	Nov 05	
Date for luminosity	Jun 02	Dec 03	Dec 05	Dec 06	

Table 4: PEP-II configuration parameters in a ongoing plan for higher luminosity. The additional rf cavities and other improvements for Steps I and II are funded; Step III represents additional investment in rf and interaction region reconfiguration under consideration.

in Figure 2. Note that this is an accelerator view of the experiment, with very different horizontal and vertical axis scales. The beams are brought into collision and then exit the IP along an S-bend orbital path. This scheme facilitates the design of shielding for the synchrotron radiation (SR) generated in the magnetic field bends. In particular, the dipole light generated by the HEB as it is brought into collision passes through the IP and is dumped over 5 m away on the far side of the interaction region, as can be seen in the upper plot in Fig. 3. Similarly, the dipole light from the LEB is absorbed on a septum mask, 2.5 m beyond the IP, as can be seen in the lower plot. This means that, for the most part, only SR induced in the quadrupole fields needs careful masking of the central beam pipe. The shielding is provided by a series of tip masks that have a minimum radius of 1.5 cm and therefore shadow the thin beryllium central section at a radius of 2.5 cm. By this careful design, the potential backgrounds from synchrotron light are minimized, so that beam particle interactions, mostly near the interaction region, are in fact the main source of backgrounds in the detector.

While this scheme has worked very well for PEP-II and *BABAR*, KEKB has successfully employed an alternative small-angle crossing scheme instead. In this case, the HEB and LEB are brought into collision with an angle of ± 11 mrad, so magnetic separation is not required near the IP. Originally there was some concern that the crossing angle would lead to additional beam-beam instability, but this has not proven to be the case in practice. At KEKB, the beams are brought straight into collision and then exit the interaction region with a bend on the far side of the IP. Without a dipole magnet near the IP, synchrotron radiation is only generated when the beams pass through quadrupole magnets off-axis. This makes synchrotron backgrounds inherently smaller, so that here too beam particle

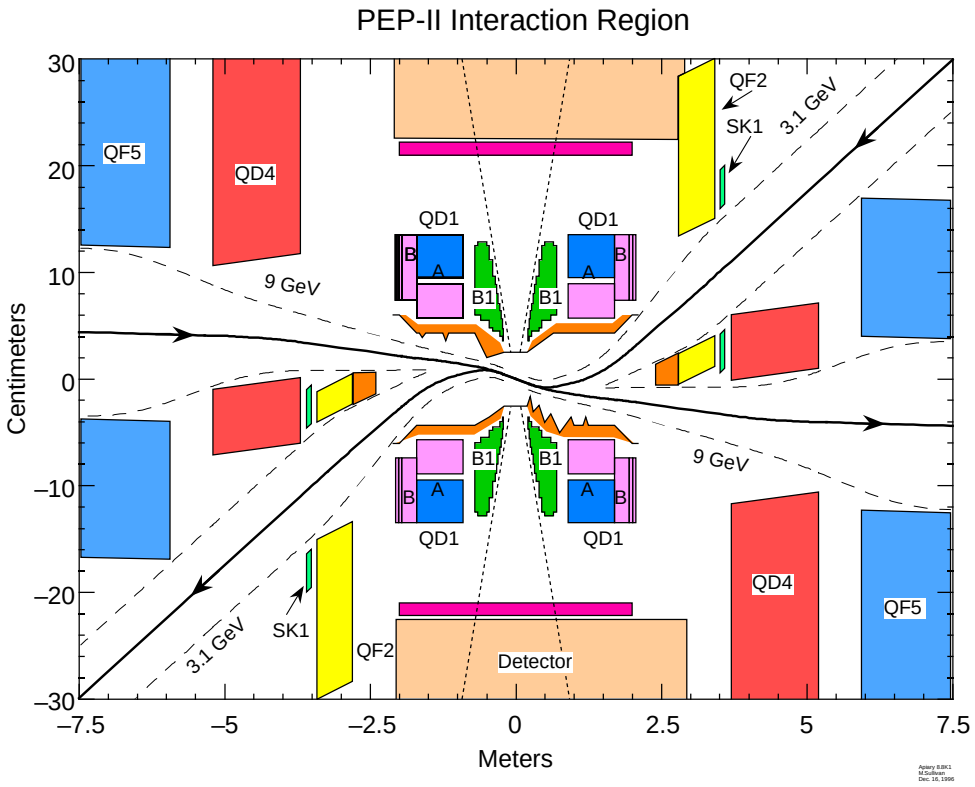

Figure 2: Schematic layout of the current PEP-II interaction region showing the S-bend configuration with zero crossing angle at the interaction point. Note the different horizontal and vertical scales.

interactions, mostly near the interaction region, are the main source of backgrounds in the detector.

The success of this small-angle crossing scheme at KEKB, suggests that a reconfiguration of the interaction region be considered as an upgrade opportunity at PEP-II. Several options along this line have been considered during a PEP-II Performance Workshop in January 2002 and subsequently in conjunction with the Task Force. The main advantage of reconfiguring the IR is the opportunity to increase the LEB focusing near the IP. In one scenario, driven in part by considerations of the IR layout for a super B Factory, a crossing angle of about 24 mrad is used with focusing provided by a superconducting quadrupole close to the IP. A more adiabatic solution is also possible, where a portion of the back end of the SmCo B1 dipole magnets is replaced with quadrupole field and the reduced dipole separation kick that results is compensated by a modest crossing angle (perhaps as small as ± 3 mrad).

During the course of our deliberations, it became clear that this more modest modification to the IR design was indeed viable. It was estimated that the PEP-II luminosity could be further improved by roughly another factor two in this scenario. The machine configuration is shown in Table 4 in the column labeled "Step III". The luminosity estimate assumes that the vertical focusing would decrease to $\beta_y^* = 4.5$ mm, with the required shorter bunch length achieved through two additional rf stations that also allow the total

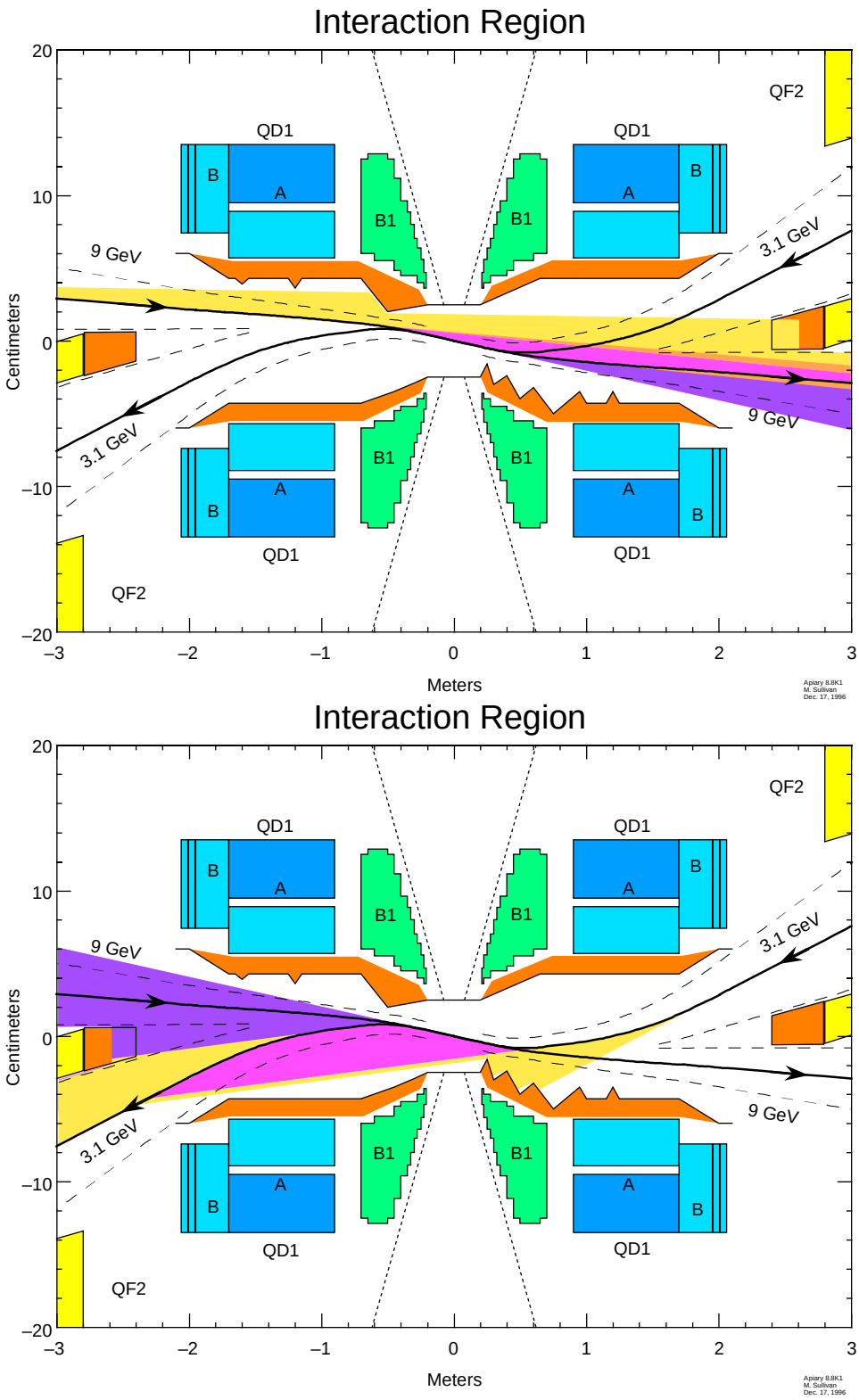

Figure 3: Synchrotron radiation sources and shielding for the high-energy (upper) and low-energy (lower) beams as they pass through the current PEP-II interaction region.

currents in the machine to be raised to 4500 (LEB) and 2000 mA (HEB) respectively. Note that at this point the LEB current is at the design limit for the LER vacuum system. The projected peak luminosity in this scenario, 4×10^{34} cm^{-2}s^{-1}, is therefore the limit of what can be accomplished by PEP-II without major new investment.

The costs of Step III in the PEP-II upgrade plan are estimated to be roughly \$12–14 million, mostly for the two additional rf stations (\$10 million). At preliminary look at the beam orbits in such a scheme indicate that it is indeed possible to match the existing lattice outside the IR region. The modest crossing angle and small displacements of the orbits relative to their present position suggests that it may not be necessary to change the SR masking scheme. In this case, the most significant effort is the design, fabrication, and installation of a set of new B1 magnets.

If installation could be coordinated with the replacement of the horizontal modules of the SVT, most likely in 2005, the amount of downtime for *BABAR* would not be significantly impacted by the IR reconfiguration. This target date also leads to the longest plausible period for integrating luminosity at 4×10^{34} cm^{-2}s^{-1}. In some scenarios it would be conceivable to reach 1.5–2 ab^{-1} by the end of the decade under these circumstances.

3.2 Detector upgrade opportunities

While a further factor of two in peak luminosity will bring significant improvement in the physics reach of *BABAR*, particularly when integrated over 3–4 years, it is conceivable that there may also be opportunities for upgrades to the detector that effectively contribute another improvement factor to the overall physics sensitivity of the experiment. The reconfiguration of the IR offers the chance to redesign aspects of the vertex detector. It may also give enough time for installation of unrelated new components, as long as they can proceed in parallel.

After three years of operation, we now have a good understanding of the performance of all *BABAR* detector systems. It was therefore possible for Group 2 to explore the range of options for detector improvement that might be worth pursuing. For this purpose, the performance of each detector system was examined with the help of system experts and possible upgrades discussed. A number of options emerged, although only two were pursued with physics studies. As already noted, we assumed that the barrel RPC replacement for the IFR would proceed on the timescale of 2004–2005, under the active direction of *BABAR* management.

Improved impact parameter resolution with a new SVT inner layer (L_0). This was the most promising opportunity, which will be discussed in detail below.

Improved angular coverage through instrumentation of B1. Since the B1 magnet is to be rebuilt in the proposed IR reconfiguration, this offers the opportunity to consider integrating instrumentation into the design so as to improve the forward angular coverage of the detector in the region between 200 and 350 mrad. We would expect that improved acceptance would be the greatest benefit to physics studies that are sensitive to

missing energy, such as $B^- \to \tau^- \overline{\nu}_\tau$. A model of the response of B1 as a calorimeter was devised to allow exploration of the physics impact of such an upgrade project.

While a good fraction of the particle backgrounds in the detector occur due to particle showers in the B1 material, we do not have a good quantitative measurement of the rate. In order to pursue further the feasibility of this option, additional instrumentation has been added to the B1 magnets during the 2002 summer shutdown. The data provided by the new instrumentation will be crucial to determining whether instrumenting B1 is at all feasible.

At present, the B1 magnet consists of 6 SmCo slices of 2.5 cm iron equivalent followed by 5 slices of 5.1 cm iron equivalent. The proposed small angle crossing scheme would lead to replacement of several of the rear dipole slices by quadrupole field. It is conceivable that detector layers could be inserted between two absorber slices without changing magnetic properties. Such a detector could be along the lines of a similar device built for L3, which consisted of lead-scintillator rings with photodiode readout. Another option would be silicon rings, which are used for the ALICE forward multiplicity detector. A close examination of the present design of B1 shows that insertions after 3 slices ($4X_0$) and 6 slices (10–$12X_0$) could be used as a veto counter to cover the region between 160 and 300 mrad. The resolution of such a device would be dominated by lateral shower leakage. We therefore assumed a energy resolution of $50\%/\sqrt{E}$ in modeling the device.

Improved angular resolution for DIRC Cherenkov photons. The single-photon angular resolution in the DIRC receives significant contributions from dispersion in transmission along the quartz bars (5.4 mrad), from imaging due the finite bar size (3.9 and 7.9 mrad in y and x), and from the size of the photomultipliers (5.8 mrad). It is conceivable that faster and smaller phototubes could be used, which would both reduce the contribution to resolution and achieve better background rejection. Proximity focused schemes have also been considered, which would lead to resolutions in the 5–7 mrad range versus the present 9.6 mrad, although with considerable angle dependence. However, it appears that the limits to DIRC performance are more related to physics tails, and tracking performance and alignment, then to DIRC photon angular measurements. The mis-identification rates are much larger than implied by the significance of the Cherenkov angle separation. Until these questions are resolved, it appears unwarranted to embark on a major and costly upgrade leading to an improved the DIRC angular resolution. Endcap coverage with a DIRC device was briefly discussed, but this does not appear practical either.

Active detection of conversions before the EMC. Despite the considerable design effort that went into reducing material in front of the EMC, there remain significant tails to the energy resolution from the calorimeter, particularly for low energy photons. Studies have shown that the energy resolution tails are noticeably worse for showers that have hits in the DIRC and efforts are underway to determine whether energy can be recovered from DIRC information. While we briefly considered the possibility of inserting a thin wire chamber device between the DIRC and the EMC in order to detect pre-showering photons, it was unclear whether this would bring any benefit over-and-above possible

recovery from the DIRC itself. In addition, the space involved is presently occupied by the source calibration system, which is an essential component of the EMC calibration system. There does not appear to be a sensible scenario for detector modifications to address the EMC resolution tails.

3.3 Scenarios for improved vertexing precision

Impact parameter resolution is determined by the resolution $\sigma_0 \sim 15\,\mu$m of the first measurement point on the track and multiple scattering contributions in the extrapolation to the IP

$$\sigma_{ms} = \frac{0.014 r\sqrt{x}}{\beta pc \sin^{5/2}\theta}\,\mathrm{cm} \tag{1}$$

where r is the extrapolation radius, x is the amount of intervening material (% radiation length), and momentum is in GeV/c. For example, a 1 GeV/c track at $\theta = 90^{\mathrm{o}}$ with a first measurement point at $r = 2.5\,$cm ($\sigma_0 = 15\,\mu$m) that is extrapolated to the IP through a double-walled beryllium beam pipe with water cooling (about 1.13% of a radiation length) will allow impact parameter (d_0, z_0) determinations with $50\,\mu$m resolution. Thus, for a fully reconstructed B meson candidate, one might expect to reconstruct the spatial position of its decay vertex to a precision of 50–100 μm, taking into account that many of its decay daughters will have momentum well under 1 GeV/c.

In the case of time-dependent asymmetry measurements, which depend on the proper time difference between the decay of a reconstructed B meson, B_{rec}, and the recoiling tagged B meson, B_{tag}, the measurement resolution for Δt does not result in significant loss of sensitivity until $\sigma(\Delta t)$ is comparable to the typical B^0-$\overline{B}^0$ oscillation length of $250\,\mu$m. The error on Δt is dominated by uncertainties in the reconstruction of the B_{tag} vertex and is found to be about $180\,\mu$m with the present SVT configuration. Thus, we do not expect a significant improvement in sensitivity here from a new inner SVT layer.

Beyond this application, there are many other situations, particularly for rare decays, where improved vertex resolution may be beneficial as a means of reducing backgrounds. For example, the hadronic daughters of a charmless B decay all originate from the B decay vertex and may be distinguishable from the much more common tree-level $b \to c$ transitions with a secondary charm vertex. In other cases where continuum background from light quark production is dominant, the vertex topology of the event may also be useful as a tool for background rejection.

	r_{BP} [cm]	Be [mm]	H_2O [mm]	Si [μm]	X_0 [%]
Current	2.5	1.3	1.5	390	1.5
Scenario I	2.0	1.0	1.0	320	1.0
Scenario II	1.5	0.8	1.5	320	0.9
Scenario III	1.0	0.5	0.0	215	0.5

Table 5: Scenarios for an upgraded SVT. Additional material in the form of gold and nickel coatings is included in the total budget for some scenarios.

Based on Eq. (1), the impact parameter resolution for charged tracks in the detector can be improved linearly by reducing the radius r of the first measurement and by a reduction in the amount of material x. Without a detailed design of the beam orbits through the IR, and an assessment of the SR produced in IR magnets and SR shielding design, it is difficult to know how far down in radius one can push the first position measurement. Therefore, we have opted to explore several scenarios that span the range from the current detector to the most aggressive conceivable. If significant gain in physics reach can be obtained with improved vertex resolution, then we can refine what can actually be achieved by balancing technical risks and constraints.

Three scenarios of this nature are provided in Table 5. They all assume that the beampipe is reduced in radius enough to allow the insertion of a new inner layer, L_0, inside the present SVT. The SVT itself would be retained intact and so the investment in the upgraded detector would be kept reasonably modest. The three scenarios allow us to explore the physics impact of beam pipes with inner radius 2.0, 1.5, or even 1.0 cm. As already noted, the tip masks that provide shielding for the beryllium beam pipe are presently at 1 cm smaller radius than the beam pipe itself. Some of the extra 1 cm space provides operational margin in terms of orbit control through the IR and could be reduced at the expense of some operational risk. The smaller radius for the first measurement layer would allow for a shorter modules, thereby also reducing the height required for shadowing. On the other hand, the dipole-induced SR from the LEB does not have much clearance with respect to the SR mask tips near the IP. Thus, Scenario III is clearly aggressive and probably not achievable. Scenarios II and I have increasing plausibility at the expense of reduced levels of impact parameter improvement.

3.4 Background projections and detector limitations

An initial assessment has been made by all systems, in an effort to understand their ability to cope with luminosities as high as 4×10^{34} cm^{-2}s^{-1} and, in particular, the projected backgrounds. Background extrapolations are based on present models of LEB, HEB, and luminosity component sources, which are then scaled to future machine currents. Background rates depend to some extent on the details of the interaction region geometry and beam orbits. A first look at the beam orbits that would be required in a small crossing-angle scheme show that the changes are modest and so extrapolation from currently observed background rates is probably a reasonable estimate. However, it should be noted that actual operational conditions can produce a wide range of observed background conditions for a given current, leading to additional uncertainty in the projections. The onset of a significant background component that scales with the square of the current could potentially pose a problem.

3.4.1 SVT projections

The largest dose rates in the SVT are received in the horizontal plane of layer 1. The worst areas of layer 2 will last about twice as long, while the rest of layer 1 should survive 5 times as long. The readout chips are the weak link. These have been tested up to 5 MRad integrated dose, and further testing is ongoing. Serious degradation is observed

at 3–4 MRad, but there is no hard failure. Instead, lower gain and higher noise occurs at a rate of about 10–20%/MRad.

Replacement modules are already available for layer 1. By 2004, the estimated integrated dose that will have been received by the existing horizontal modules is about 3.2 MRad, based on the luminosity upgrade plan. This rises to 4.4 MRad by 2005. Thus, there is likely to be noticeable degradation in layer 1 performance in the horizontal plane by the time of the planned replacement in the summer of 2005.

For peak luminosities in the range 2–4 $\times 10^{34}$ cm^{-2}s^{-1} the midplane dose rate rises to about 1.5–1.9 MRad/year, based on scaling with the planned currents. This implies that the high dose region of layer 1 might only be serviceable for a further 2 years, even after replacement in 2005. Clearly, this is a potential problem. However, one should recall that the corresponding layer 2 horizontal modules will likely be usable for 4 years and the rest of layer 1 for 10 years. If the SVT continues to operate in this condition, the degradation of impact-parameter resolution for single tracks will be minimal and confined to a small azimuthal range. It is not clear how significant the effect would be for B vertex reconstruction or the Δt measurement, since vertex reconstruction involves a number of tracks not all of which would be degraded. It is conceivable that the performance loss could be acceptably small.

Further study of options, including the difficulties of simply rotating the SVT itself, and the potential impact on physics appears to be warranted. There do not appear to be particular DAQ issues for the SVT, even at the highest luminosities.

3.4.2 DCH projections

Based on the July 2000 background measurements or the trigger group's model, the DCH backgrounds are projected to result in 530 useful hits (800 raw hits) per event at the maximum luminosity. Thus, there will be an average occupancy of about 11%, which should be manageable. Since there is no strong radial or azimuthal variation in the background rates, there should be no particular area of the chamber that experiences a problem. An additional 10 hits in each of the first four layers (96 cells) will probably not have a serious impact on tracking efficiency or trigger. There are occasional examples of 1–2 full FEA readout modules, which introduces deadtime due to the resulting long readout time. Visually, these events appear to be cases of tightly spiraling conversion pairs, although it is not possible to definitively demonstrate this conclusion. We address the question of DAQ limitations below.

3.4.3 DIRC projections

Backgrounds in the DIRC are dominated by single photoelectrons produced by soft photons interacting with the SOB water. The main issue is the total DAQ throughput, rather than pattern recognition or separation performance. The background rates are quite sensitive to machine tunes. Dedicated work on identifying hot spots and installing localized beam shielding has already reduced the rate by a factor of 10 since turnon. Further improvements are possible and shielding design should be incorporated in any major redesign of the IR. Luminosity-dependent background terms will dominate for peak lum-

nosities above 1×10^{34} cm^{-2}s^{-1}. The quartz bars themselves are radiation hard and do not present a problem in terms of integrated radiation dose. The projected DAQ rates for the DIRC are 300 (530) kHz for the currents required to produce peak luminosities of 2 (4)$\times 10^{34}$ cm^{-2}s^{-1}. With the recent replacement of the DIRC TDC chips, the DIRC readout is able to handle rates up to about 1 MHz with small deadtime. Thus, the DIRC should operate at the maximum luminosities with performance essentially unchanged from that at present.

3.4.4 EMC projections

There are two general issues relating to backgrounds in the EMC. The first is radiation damage to the CsI(Tl) crystals, resulting in a loss of uniformity and reduction in overall light yield with time and an associated reduction in the energy resolution. To date, the EMC has integrated approximately 4–7% of the lifetime integrated dose limit of 10 kRad with a typical dose rate of 4–9 Rad/fb^{-1}. The highest dose rates occur in the innermost rings of the endcap, particularly in the horizontal plane. Significantly lower rates are observed in regions of the central barrel. It is not clear at this point what fraction of the dose is attributable to injection and how much is accumulated during stable beams, but unless the beam lifetimes were to significantly decrease over the next few years (implying higher particle loss rates and therefore requiring higher injection rates) we would not expect a significant increase in the dose/fb^{-1} in any scenario in which the detector could reasonably collect data. A naive extrapolation of the dose rate would therefore suggest that regions of the endcap would exceed their nominal lifetime dose sometime around 2007-2008, potentially resulting in a significant degradation of the cluster energy resolution in this region. The barrel region will likely integrate only about half of its lifetime dose within this same period. It is not clear whether or not this would have a serious impact on physics performance.

The second EMC background issue is the occupancy due to background photons, which have the effect of either producing spurious neutral clusters or degrading the quality of clusters from "physics" sources due to overlap with low-energy background photons. A naive extrapolation of the observed single-digi occupancy to luminosities of 2–4$\times 10^{34}$ implies an occupancy of $\sim$ 50%, dominated by a background component which scales with luminosity rather than the single beam currents. Moreover, we would naively expect 5–8 reconstructed EMC clusters per event with energy $E > 30\,\mathrm{MeV}$ resulting from background sources (compared with ~ 7 from "physics" events). This would potentially lead to a significant combinatorial background, for example to π^0 reconstruction, and a degradation of the energy resolution of clusters, which could for example impact electron ID performance or the π^0 mass resolution.

Nevertheless, based on these findings, no substantial upgrades are planned for the EMC within the timescale considered for this report. Possible remediation measures include increasing the EMC digi energy threshold and/or modification of the cluster reconstruction algorithm, with some tradeoff in EMC physics performance.

3.4.5 IFR projections

While there are plans to change the technology employed for the barrel portion of the IFR, we can use measurements of present background conditions to project rates and understand sources. The rate limit set by the current front-end card (FEC) is 80 kHz or 30 Hz/cm^2; however the RPCs themselves will likely experience aging problems that will be more limiting.

Overall rates in the external layers of the forward endcap differ by more than an order of magnitude from internal layers. The main source of background in the external layers is beam related, while layers 15 and below are mainly due to IR sources. Beam backgrounds from the HEB mainly affect layer 18, while the LEB backgrounds extend down to layer 15. There is evidence that the outer forward endcap backgrounds are dominated by the LEB scraping upstream collimators. Unfortunately, both the counts in beam loss monitors near the collimators and the singles rates for the outer layers show a quadratic dependence on the LEB current. Should this hold for future projections, then we estimate that there will be nearly a factor of 10 increase in background rates in the outer endcap at 4×10^{34} cm^{-2}s^{-1}. This suggests that layer 18 will be unusable and probably layer 17 as well.

Background rates in the interior layers of the endcap scale linearly with luminosity, which implies an average of about 10 Hz/cm^2 at the maximum luminosity. However, the distribution is not uniform across the RPCs; instead it is concentrated in the region around the beam pipe. Maximum values are presently around 1.5–2 kHz/strip or 5 Hz/cm^2. Thus, it appears that there will be background problems for the interior layers of the endcap as well, in the region near the beam pipe.

The singles rates for barrel RPCs also show a linear dependence with luminosity at present currents. A positive slope is observed for inner layers and layer 18, while all other layers show essentially no dependence with luminosity. The worst case dependence is observed to be about 1.5 kHz/10^{33} cm^{-2}s^{-1}. This projects to 60 kHz/module or 3 Hz/cm^2 at 4×10^{34} cm^{-2}s^{-1}. Since there are no significant non-uniformities, the barrel IFR should be able to tolerate backgrounds at the projected maximum luminosities. If the barrel RPCs are replaced with LSTs, this conclusion remains unchanged.

3.4.6 DAQ and trigger projections

The existing simulation of DAQ throughput and rate capability has been used to extrapolate conditions at LEB (HEB) currents of 4500 (2000) mA. These simulations continue to show that there are several bottlenecks in the DAQ for the DCH, which will limit the overall DAQ rate at about 4 kHz: the DCH optical Glink fibers (3.8 kHz), feature extraction (3.4 kHz), and fragment-level slot-0 ROMs (3.8 kHz). The next limit is the EMC feature extraction code, but this does not become a factor until a 6 kHz DAQ rate. Based on nominal L1 trigger rate projections for 2 (4)$\times 10^{34}$ cm^{-2}s^{-1}, this limitation would result in 3–8% (15–30%) deadtime for twice the nominal extrapolation of the 2001 or 2002 background conditions.

Based on February 2002 background model, and incorporating a 40% rate of rejection for background triggers due to the DCT upgrade, the projected trigger rates shown in

Currents		Luminosity	Rates [Hz]		
HEB (A)	LEB (A)	$\times 10^{33}$ cm^{-2}s^{-1}	Nominal	Luminosity	2× Background
1.8	3.6	20	2550	1400	3570
2.0	4.5	40	4260	2800	5600

Table 6: Projected trigger rates for upgraded luminosity. The nominal rate includes both luminosity and background components. Doubling the background rates to allow headroom gives the last column.

Table 6 are obtained. We find that the L1 rate will be near the DCH-imposed limit for the DAQ rate at 2×10^{34} cm^{-2}s^{-1}, but will potentially pose a problem at 4×10^{34} cm^{-2}s^{-1}. There are a number of options available for addressing this problem.

Modify DCH readout electronics. The serial transfer of any full FEA box (180 channels) sets the limit for the DCH readout at about 240 μs. Further subdivision of physical FEA boxes into readout groups with a maximum of 96 channels may be possible, leading to a doubling of the number of Glink data fibers and a reduction of the maximum transfer time to 130 μs. This would also allow a doubling of ROMs, relieving the feature extraction and slot-0 ROM limitations. The feasibility and scope of such a project has not been seriously investigated from an engineering standpoint. If this is indeed an attractive and viable option, it is likely that it could be implemented in about one year.

Tighten the L1 trigger. The impact of two options has been examined. A tighter control of EMT trigger lines could yield a 15% background rejection, reducing the L1 rate by 0.5-1.0 kHz for maximum luminosity with some loss of tau-pair events. Further improvement to the Bhabha veto, through upgrades to the EMT and GLT, may be able to reject 40% out of 53 nb of the Bhabha cross section. This would reduce the L1 rate by about 1 kHz. Thus, it may be possible to keep the L1 rate at or below 4 kHz, including a factor of two margin for backgrounds. Such a smaller L1 rate would also have benefits for reduced computing and storage requirements after the data are acquired.

In either of these scenarios there is time to further evaluate projections of background conditions and trigger rates. There is a possibility that the DCH payload can be reduced by changes to the front-end optimization; however, factors of two improvement are unlikely.

4 Simulation tools

To establish the expected physics reach of upgraded versions of the *BABAR* detector we have developed a fast Monte Carlo simulation tool that employs an easily modifiable, text based, geometry description. This development was necessary because the speed of the *BABAR* full simulation (roughly 1 s/ev) is not suited to generating a large data sample in a short time; in addition, changing the detailed geometrical description of the detector

is a fairly involved and complex process, which cannot be implemented easily for several detector configurations.

4.1 Pravda/Trackerr tool

The fast MC was assembled by simply merging two existing packages: PravdaMC [1] and Trackerr [2]. PravdaMC provides a mechanism inside of Beta to smear generator level particles and produce lists of pseudo–reconstructed BtaCandidates, which can then be fed to existing analysis packages. In the original PravdaMC implementation the amount of smearing is given by a formula, and correlations between errors are not taken into account. Trackerr is a FORTRAN program that, starting from a text based detector description file, can calculate the reconstruction errors on tracks of given momentum and angle, including the full correlation matrix.

The PravdaMC/Trackerr interface we developed uses the errors calculated by Trackerr to smear the charged tracks parameters within the framework provided by PravdaMC. In this way, different detector configurations can be readily simulated with different MC samples and then analyzed with existing analysis packages.

The program can be used in two modes: (1) the event generator is used to produce the events that are then processed by Pravda; or (2) events are read from an existing MC collection and the MC truth tracks are passed to Pravda for processing. With the former method it is possible to generate much higher statistics than available in SP4, while with the latter method one can make a direct comparison between the full MC and Pravda with the same events.

The interface uses the `f2c` [3] program and include files to transfer program flow and information between the C++-based Beta framework and the FORTRAN-based Trackerr program. For each charged track, the MC-truth track parameters are passed to Trackerr, which calculates the intersection of the track with the active layers defined in the geometry file. By construction, the geometry is specified with a rotational symmetry around the z axis. The errors assigned to each hit take into account the angle of the measurement with respect to the z-axis, as well as an angle-related degradation factor. Energy loss of the particle in the detector material is taken into account only in calculating the total path length, *i.e.,* no adjustment is made to the trajectory and particles always follow perfect helices. The hits are then used to propagate the track error matrix to the origin, based on a method described by Billoir [4].

The smeared parameters are calculated with the following procedure: the error matrix is diagonalized and parameter variations are thrown from Gaussian distributions in the error matrix diagonal space; the variations are transformed back to the physical parameter space where they are passed to the Pravda framework; Pravda adds the contribution to the MC truth value to obtain the smeared parameters and associates the full error matrix to each track.

4.2 Detector modeling

The Trackerr representation of the *BABAR* SVT and Drift Chamber can be seen in Fig. 4. The SVT modules are represented by 390 μm equivalent thickness of silicon, which takes

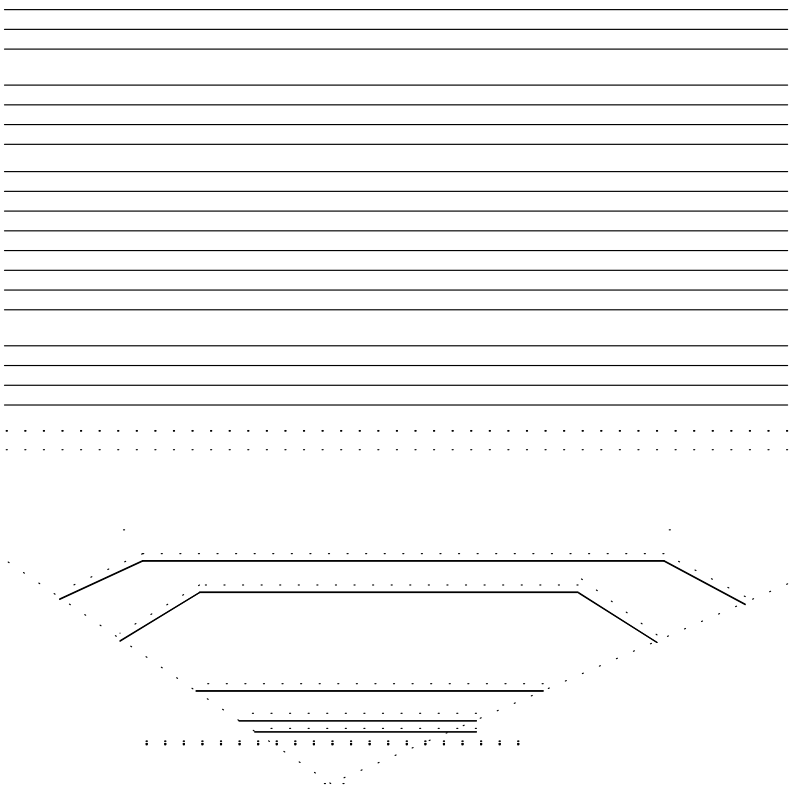

Figure 4: Trackerr representation of the current *BABAR* detector. Continuous lines represent active material, while dotted lines represent inactive materials.

into account the crossing angle and the extra material introduced by the fanout readout. In addition, the mechanical structure is modeled as a 100 μm-thick uniform layer of carbon fiber.

The point resolution is modeled with a quadratic form $\sigma = \sigma_0(1 + p_1\theta + p_2\theta^2)$ where θ is the particle's incident angle with respect to the wafer normal and the parameters σ_0, p_1 and p_2 are fitted from the data. The resolution data are shown along with the fits in Fig. 5, while the parameters used in the model are listed in Table 7.

The Drift Chamber is modeled with 40 layers of a material equivalent to the gas-wire mixture, spaced according to the DCH design. Each layer has an equivalent thickness of $4 \times 10^{-5} X_0$ and a resolution of 140 μm. The support tube, inner and outer cylinder of the DCH have equivalent thicknesses of 0.05%, 0.3% and 1.5% respectively.

The parameters used to represent a track are the standard *BABAR* set

d_0**:** The distance in the $x - y$ plane from the origin of the orbit (cm).

ϕ_0**:** The azimuthal angle corresponding to the track direction in the $x - y$ plane (rads).

ω**:** The signed geometrical curvature $\omega = 1/r$ (cm^{-1}).

z_0**:** The z position of the orbit at the point of closest approach in the $x - y$ plane.

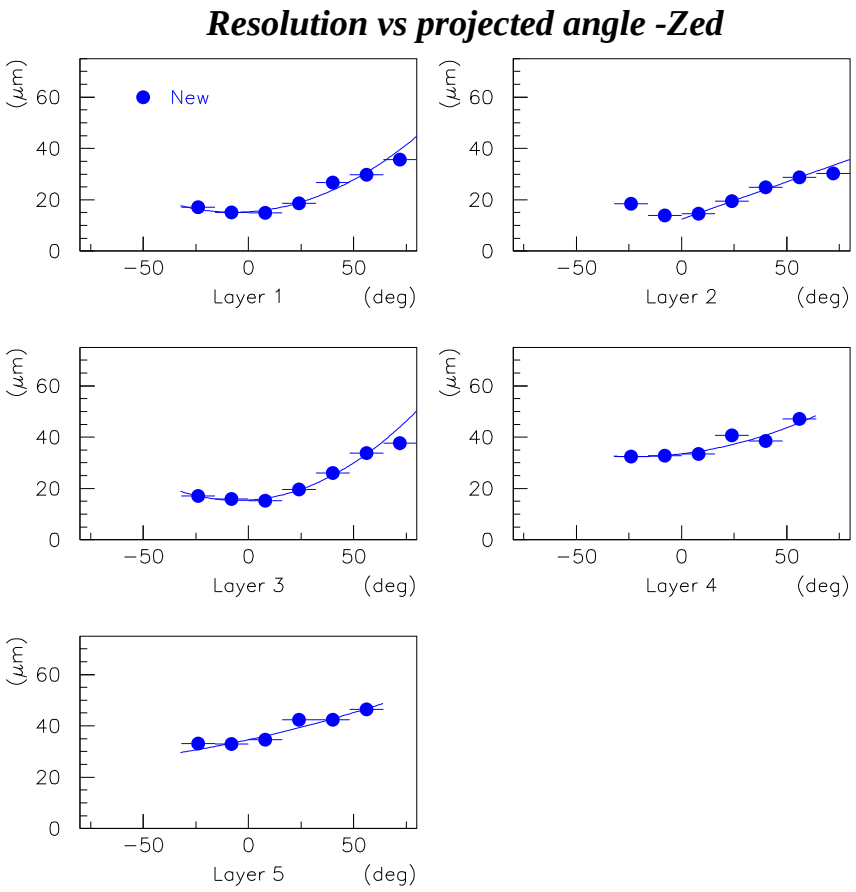

Figure 5: Fit to the angular dependence of the SVT point resolution for the z-measuring strips.

$\tan\lambda$**:** The tangent of the dip angle.

For a more detailed description along with sign conventions see Ref. [5].

The calculated resolution on the track parameters is shown in Fig. 6 as a function of $\sin\lambda$ for various momenta. It agrees reasonably well with the data [6], shown in Fig. 7, and with the full Monte Carlo, as discussed in the following section.

4.3 Validation

The accuracy with which the Pravda/Trackerr Monte Carlo reproduces the detector performance is necessarily limited by the relative crudeness of Trackerr's detector representation. We have studied the level of agreement between fast simulation and the full Monte Carlo with a common set of SP4 simulation data. For this purpose, the MC truth information is smeared using Trackerr, and then compared with the corresponding fully simulated and reconstructed quantities. The comparison has been done both track by track and statistically with the ensemble of charged tracks.

The error distribution for the five tracking parameters as obtained from the SP4

Layer	ϕ			z		
	σ_0 [μm]	p_1	p_2	σ_0 [μm]	p_1	p_2
1	13	1.5	0	15	0.2	0.8
2	13	1.5	0	15	0.2	0.8
3	20	1.5	0	15	0.2	0.8
4	18	1.5	0	35	0.2	0.2
5	18	1.5	0	35	0.2	0.2

Table 7: Fitted values to the parameters describing the angular dependence of the SVT point resolution with the parameterization $\sigma = \sigma_0(1 + p_1\theta + p_2\theta^2)$.

simulation is shown in Fig. 8 for generic $B\overline{B}$ decays, while the errors predicted by the Trackerr for the same events are shown in Fig. 9. Table 8 summarizes the average errors and shows that the agreement between full simulation and fast smearing is at the level 20-25%, which is considered adequate for the goals of the present study.

Parameter	Full MC	Fast MC	Full MC/Fast MC
d_0	0.022	0.019	1.16
ϕ_0	0.0072	0.0067	1.075
ω	7.5×10^{-5}	8×10^{-5}	0.937
z_0	0.036	0.029	1.241
$\tan\lambda$	0.012	0.011	1.091

Table 8: Comparison of average tracking errors obtained for generic $B\overline{B}$ decays with the GEANT4 simulation (Full MC) and Trackerr/Pravda (Fast MC).

The correlation matrix terms are also in relatively good agreement, except for d_0 and z_0, which show 20–25% discrepancies that are not fully understood. Since these differences have a negligible impact on vertex reconstruction, we have not pursued the problem further.

5 Impact of detector upgrade options

The main detector upgrade under consideration is the addition of a new silicon layer at a radius inside the present SVT. The improvement in impact parameter resolution has been studied, as well as any benefits for the resolution on Δt. New possibilities for tagging algorithms are also examined.

5.1 Resolution for track parameters

The impact of reducing the beam pipe radius, which allows the addition of a small radius layer (L_0) to the current SVT, has been studied both in terms of single track parameters and vertex resolution.

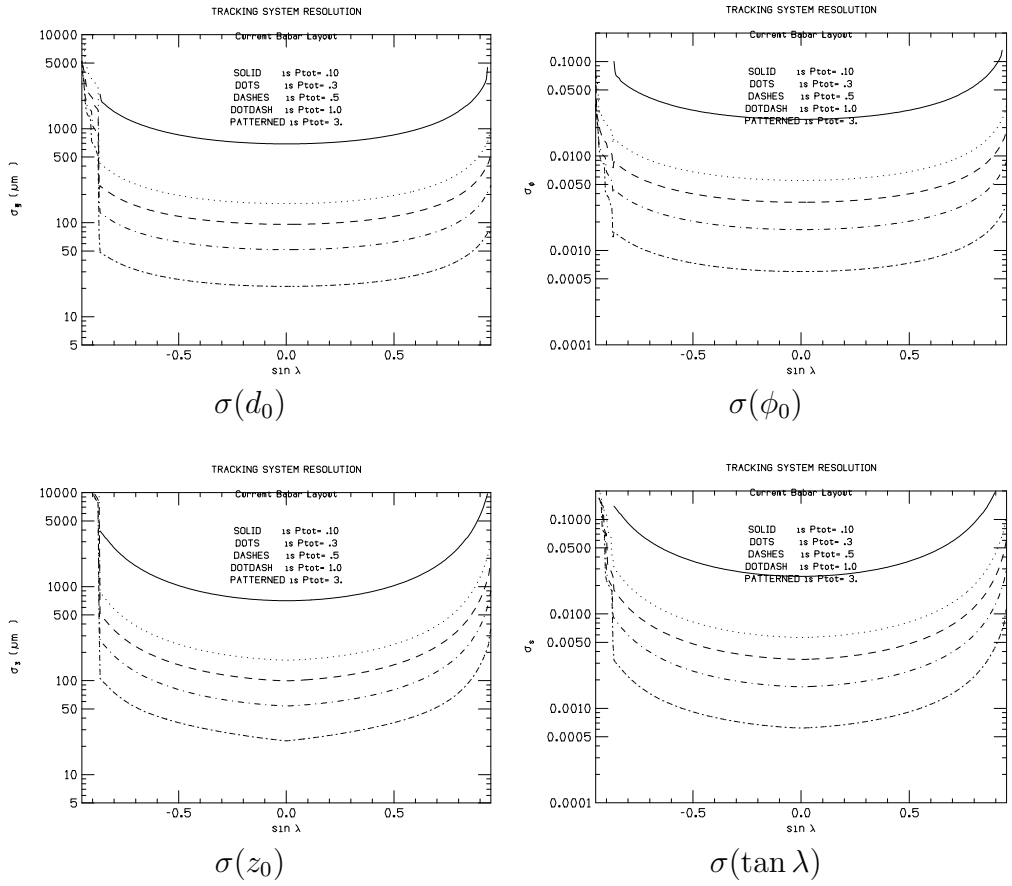

Figure 6: Track parameter resolutions vs. dip angle for different momenta.

The single track parameters most affected by such an upgraded SVT are, as expected, the distance of closest approach in the xy plane (d_0) and in the z direction (z_0). As already noted, the resolution for these two parameters is directly related to the radius of the first layer and the amount of material in front (and including) the first measurement. For our momentum range the point resolution of the first measurement is typically negligible compared to the contribution of multiple scattering.

Using the Trackerr/Pravda interface described Section 4, we have studied both generic $B\overline{B}$ events and $B^0 \to J/\psi K^0_S$ decays, obtaining similar results. The three upgraded models that have been considered are described in Section 3.3. Table 9 summarizes the observed performance improvement in generic $B\overline{B}$ events for the five track parameters. The corresponding distributions of errors for the three upgrade scenarios are provided in Figures 10 and 11. As expected the impact parameter measurement is most improved; the resolution is reduced by factors of about 1.5, 2 and 3 for beam pipe radii of 2.0, 1.5, and 1.0 cm respectively. Some more modest improvement in the angular resolutions is also evident along with perhaps a 10% effect on the error for the curvature measurement.

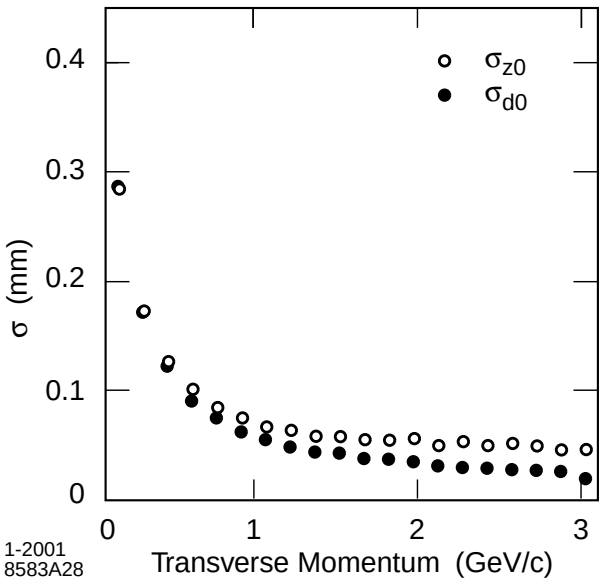

Figure 7: Resolution on the parameters d_0 and z_0 measured from data for tracks in multihadron events.

5.2 Resolution for proper time difference

The benefit of the improved impact parameter resolution for time-dependent asymmetry measurements has been studied with a sample of 2000 $B\overline{B}$ signal events with the *CP* channel $B^0 \to J/\psi\, K^0_S(\to \pi^+\pi^-)$. These events were originally produced with the GEANT MC (SP4), but are reused with the Trackerr/Pravda MC for this study.

The difference between B decay times $\Delta t = t_{\rm rec} - t_{\rm tag}$ in these events is determined from the measured separation Δz between the vertex of the reconstructed B meson ($B_{\rm rec}$), in this case $J/\psi\, K^0_S$, and the vertex of the daughters of the flavor-tagging B meson ($B_{\rm tag}$) along the z axis. Neglecting the B momentum in the $\Upsilon(4S)$ frame, one can obtain $\Delta t = \Delta z/\langle\beta\gamma c\rangle$, where $\beta\gamma$ is the $\Upsilon(4S)$ boost factor. The Δz resolution is dominated by the z position resolution for the $B_{\rm tag}$ vertex.

	Full MC	Fast MC				Full MC/Fast MC			
	(SP4)	2.5	2.0	1.5	1.0	2.5	2.0	1.5	1.0
d_0 [μm]	22	19	13	9.3	6.0	1.16	1.5	2.0	3.2
ϕ_0 [mr]	7.2	6.7	5.8	5.5	4.2	1.08	1.2	1.2	1.6
ω $\times 10^{-5}$	7.5	8.0	7.8	7.7	7.2	0.94	1.0	1.0	1.1
z_0 [μm]	36	29	21	15	9.5	1.24	1.4	1.9	3.1
$\tan\lambda$ [$\times 10^{-3}$]	12	11	9.1	10	6.6	1.09	1.2	1.1	1.7

Table 9: Track parameter resolutions obtained with GEANT4 simulation (Full MC) and Trackerr/Pravda (Fast MC) for generic $B\overline{B}$ events. The current and upgraded SVT configurations are labeled by the beam pipe radius.

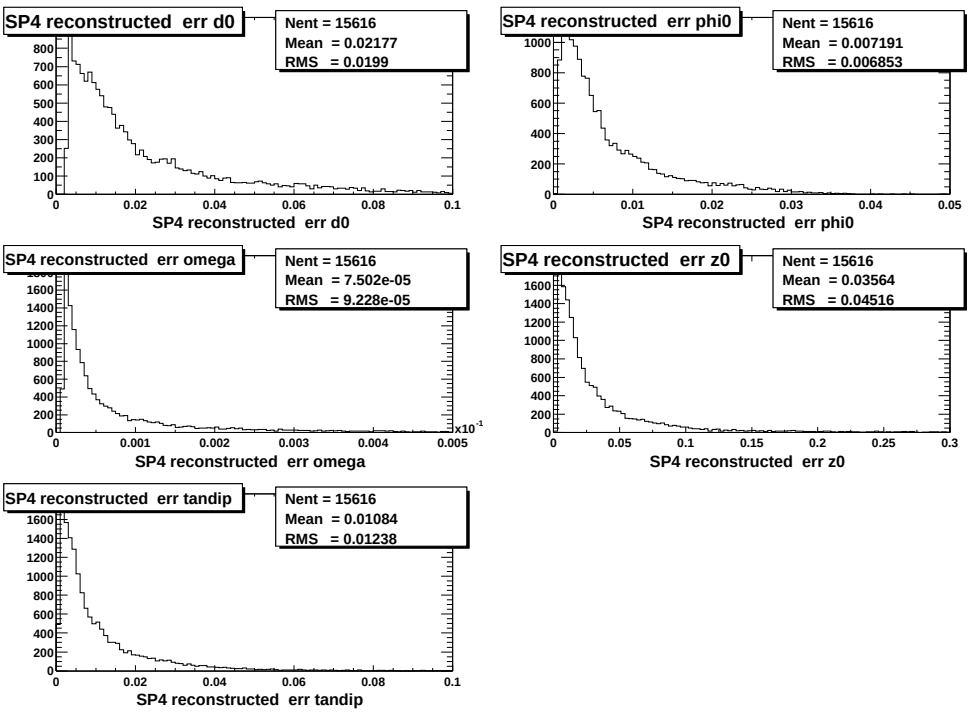

Figure 8: Resolution for tracking parameters in generic $B\overline{B}$ events, obtained with the GEANT4 simulation (SP4).

The simplest extrapolation of improvements to Δt resolution is to measure the impact based on the present algorithm. The $B_{\rm rec}$ vertex is obtained from a straightforward fit to the spatial point of origin of its charged daughter tracks. The vertex for the $B_{\rm tag}$ decay is constructed from all tracks in the event except the daughters of $B_{\rm rec}$. Since one of the two B mesons in the event is fully reconstructed, an additional constraint is available from the inferred $B_{\rm tag}$ production point and three-momentum, with its associated error matrix. This is determined from the knowledge of the three momentum of the fully reconstructed $B_{\rm rec}$ candidate, its decay vertex and error matrix, and from the knowledge of the average position of the interaction point and the $\Upsilon(4S)$ average boost. In order to reduce bias and tails due to long-lived particles, K^0_S and Λ^0 candidates are used as input to the fit in place of their daughters. In addition, tracks consistent with photon conversions ($\gamma \to e^+e^-$) are excluded. To reduce contributions from charm decay products, which bias the determination of the vertex position, the track with the largest vertex χ^2 contribution greater than 6 is removed and the fit is redone until no track fails the χ^2 requirement.

The result of the application of this algorithm in summarized in Table 10. Figure 12 shows the Δt residuals and residuals normalized to the calculated errors for the Trackerr/Pravda simulation in the 1.5 cm beam pipe scenario. We observe a substantial improvement in the $B_{\rm rec}$ vertex resolution, a more modest improvement in the $B_{\rm tag}$ vertex resolution, and about a 26% improvement in Δt resolution for this scenario. However, since the current Δt resolution is substantially better than the average B^0-$\overline{B}^0$ oscillation length of 260 μm, the improvement in sensitivity for sin2β is actually a quite small 3 (5)%

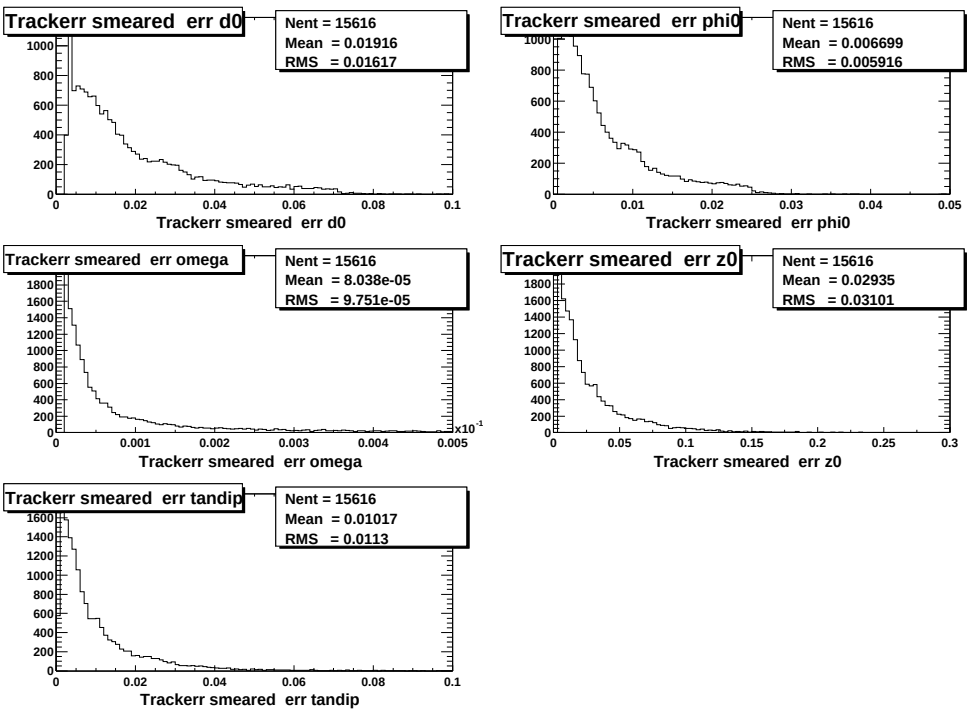

Figure 9: Resolution for tracking parameters in generic $B\overline{B}$ events, obtained with Trackerr smearing for the current SVT beam pipe of 2.5 cm.

for the 2.0 (1.5) cm upgrade.

On the other hand, given the substantial improvement in impact resolution that would be possible in certain upgrade scenarios, it is natural to ask whether the current algorithms for determining Δt remain suitable. In particular, an approach that tries to form two separate vertices on the tag side of the event may both improve resolution and reduce the charm bias. The algorithm we have attempted proceeds as follows. All combinations of tracks assignments to two vertices are identified, where the B vertex uses the same constraints as the current algorithm and a simple vertex fit is applied to the candidates for the secondary decay. No information from the secondary vertex is applied to the B vertex. From the set of all possible two-vertex assignments, we select the one with the best global $\chi^2 = \chi^2_B + \chi^2_D$. The resulting residual Δt distribution based on the $B_{\rm rec}$ and primary $B_{\rm tag}$ vertex is shown in Fig. 12. The average number of tracks participating in the primary tagging vertex is reduced from 4.4 for the standard algorithm to 2.9 for this two-vertex approach. We conclude that the vertex resolution improvements are not good enough to allow efficient separation of B and D vertices on an event-by-event basis.

5.3 Tagging algorithms and efficiencies

The present algorithms for flavor tagging of B decays is based on particle identification and kinematic information, which attempts to exploit inclusively several recognizable decay topologies that tag the state of the b quark at the time of the B meson decay. The

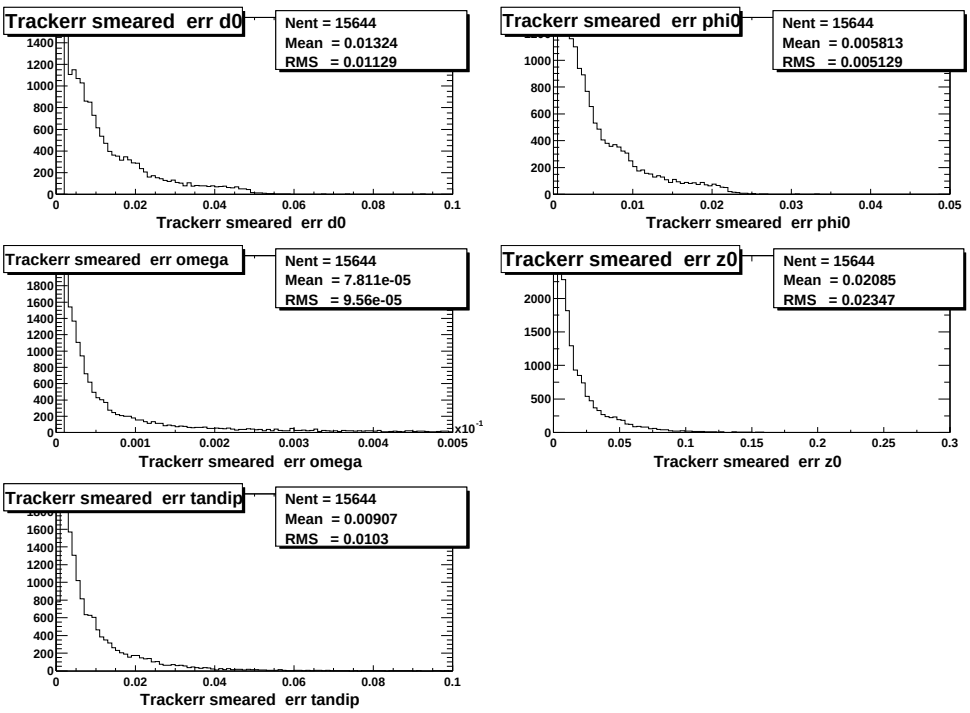

Figure 10: Resolution for tracking parameters in generic $B\overline{B}$ events, obtained with Trackerr smearing for SVT upgrade scenario I with beam pipe reduced to 2.0 cm.

figure of merit for tagging is the effective tagging efficiency $Q = \epsilon(1-2w)^2$, where ϵ is the fraction of tagged events with a reconstructed tag vertex. With the present algorithm we measure $Q = 28.1 \pm 0.7\%$ in data. Monte Carlo simulation predicts a somewhat higher efficiency of $30.3 \pm 0.2\%$, partly due to deficiencies in the modeling of the underlying inclusive charm rates.

Although the possibility of including vertexing information has been considered as a possible means of further enhancing tagging performance, only small gains have been observed that are offset by the danger of introducing unwanted correlations with the Δz determination. However, an improved vertex detector might change this situation significantly. In particular, the ability to identify the decay vertices of D mesons would allow a new topological tagging algorithm based on the recognition of secondary vertices, with the potential for large improvement of the tagging performance.

In order to evaluate the potential for improvement, we conducted a study [7] of the charm topology of B decays and then made an estimate of the efficiency for reconstructing the relevant secondary charm vertex. The study shows that the channel $B^0 \to D^- X$ is the most promising candidate for application of such a topological vertex algorithm. Assuming a perfect vertex detector, we would gain $\delta Q = 17.6\%$. Similarly, $\delta Q = 3.7\%$ would be possible with $B^0 \to D^- \ell X$ events. An realistic estimate needs to account for the probability for correctly reconstructing the secondary charm vertices. A rough estimate is obtained by assuming the D^- needs to fly a minimum of 100 μm to be found and then can be reconstructed with an efficiency of 90% thereafter. We also assume an 80% efficiency

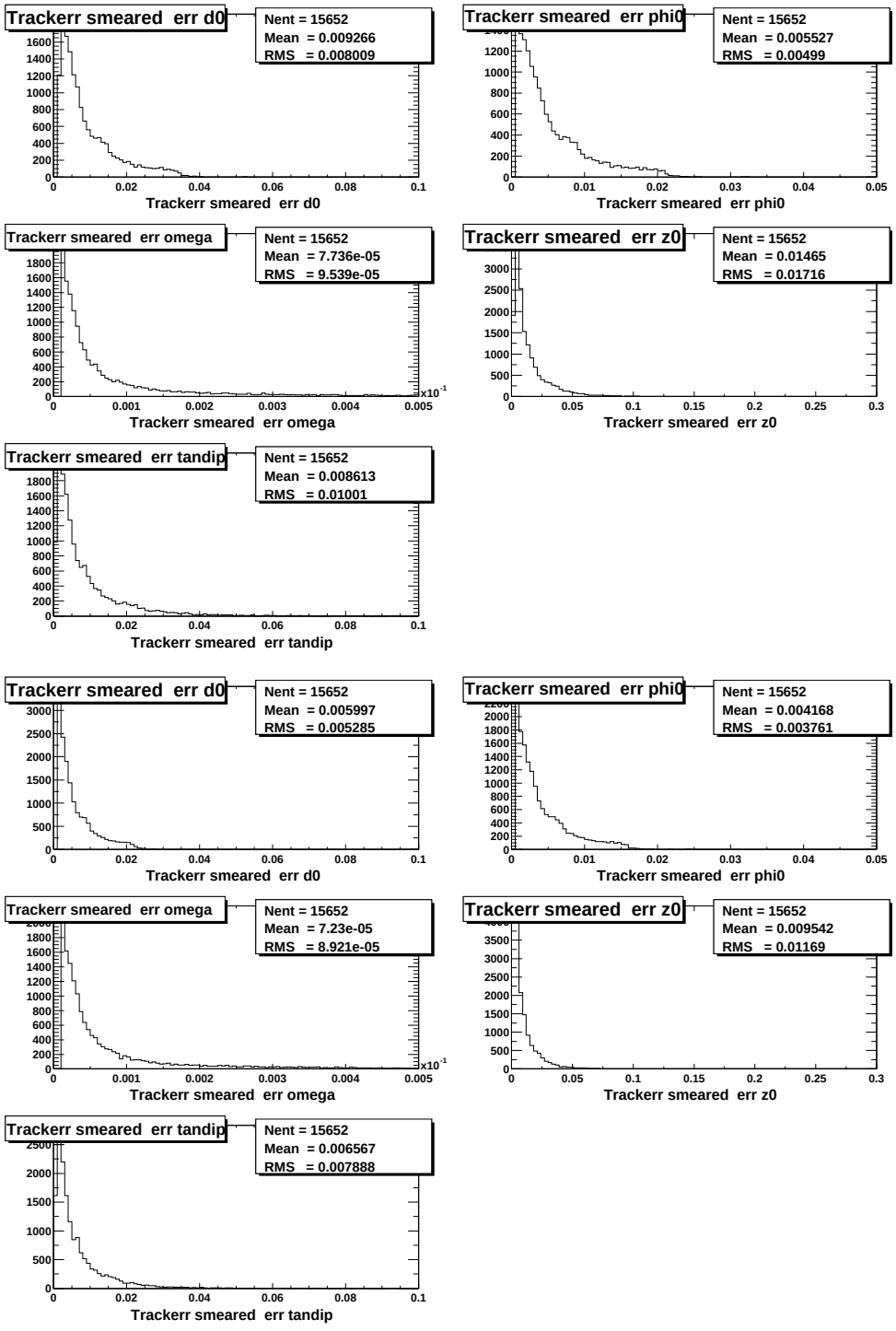

Figure 11: Resolution for tracking parameters in generic $B\overline{B}$ events, obtained with Trackerr smearing for SVT upgrade Scenario II with beam pipe reduced to 1.5 cm (upper) and Scenario III with beam pipe reduced to 1.0 cm (lower).

	Current [μm]	Improvement factor	
		$r_{BP} = 2.0\,\mathrm{cm}$	$r_{BP} = 1.5\,\mathrm{cm}$
$\sigma(x_{rec})$	45.2	1.33	1.84
$\sigma(y_{rec})$	45.1	1.42	1.92
$\sigma(z_{rec})$	45.1	1.43	1.94
$\sigma(x_{tag})$	70.4	1.23	1.55
$\sigma(y_{tag})$	33.4	1.21	1.54
$\sigma(z_{tag})$	98.0	1.12	1.38
$\sigma(\Delta t)$	0.82	1.06	1.26
Bias $\delta(\Delta t)$	-0.20	1.25	1.33

Table 10: Comparison of current $B_{\rm rec}$ and $B_{\rm tag}$ vertex resolutions, and resultant Δt resolution and bias, to the improved performance expected under SVT upgrade scenarios. The standard sin2β algorithms have been applied in this study.

for correctly reconstructing the charge. On this basis, a somewhat optimistic estimate of $\delta Q = 5\%$ could be achieved in an upgraded detector. Varying the underlying efficiency assumptions, can lead to an increase in absolute tagging performance that ranges from zero to 10%.

6 Physics projections with present and upgraded detectors

Sensitivity projections for benchmark channels have been determined for both the present detector configuration and, in relevant cases, for the upgrades under consideration.

6.1 Measurement projections for $\sin 2\beta$

6.1.1 Type I modes: $b \to c\overline{c}s$

The following assumptions have been made in projecting errors on the sin2β measurement:

- The statistical error from $J/\psi\, K^0_S(K^0_S \to \pi^+\pi^-)$ alone is 0.084 for 940 signal events, based on the summer 2002 sin2β publication [8].
- The yield of tagged $J/\psi\, K^0_S$ is about 11.7 signal candidates per fb^{-1}.
- The statistical error for the measurement with all golden modes or all golden modes and $J/\psi\, K^0_L$ scales relative to $J/\psi\, K^0_S$ alone by factors of 0.88 and 0.80 respectively.
- The statistical error for the Lepton and Kaon I tags alone is 1.53 and 1.61 times that for all tags respectively.

A detailed account of the projections for systematic errors is also provided in Table 12. Several comments are in order:

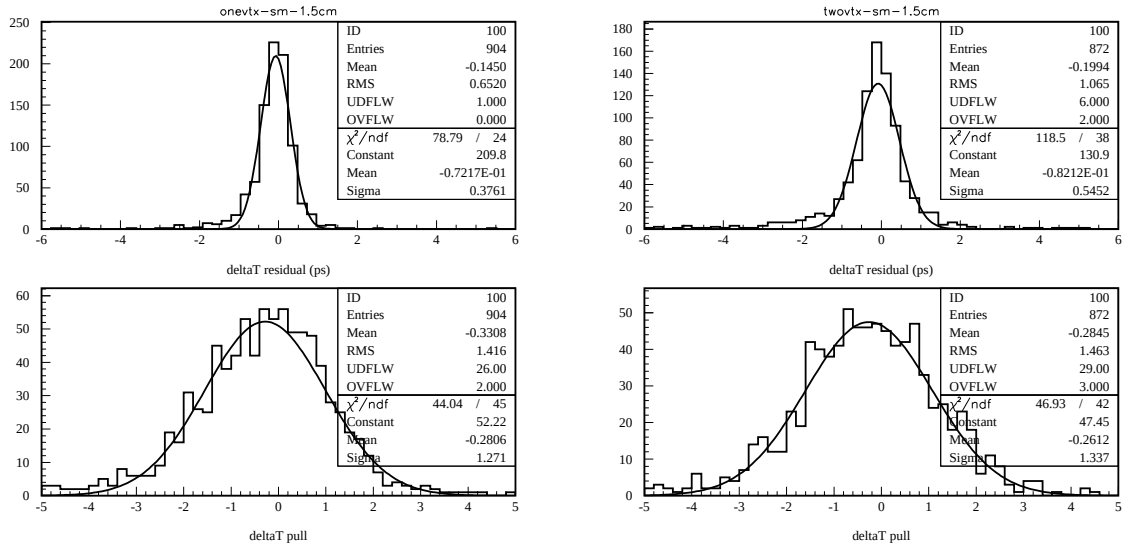

Figure 12: Distribution of the Δt residuals (top) and the residuals normalized to the calculated errors (bottom) obtained by applying the standard algorithm for an upgraded SVT with $r_{BP} = 1.5\,\mathrm{cm}$ (left pair) or the two-vertex algorithm for an upgraded SVT with $r_{BP} = 1.5\,\mathrm{cm}$ (right pair).

- **Ultimate precision:** The last column is an estimate of the systematic error that would be achievable with $50.0\,\mathrm{ab}^{-1}$ based on the cleanest tagging category alone (Leptons), where systematics from tagging are negligible and the resolution functions have much smaller tails.

- **Δt resolutions:** The largest contributions are residual SVT mis-alignments and uncertainties in the beam spot location. Both of these can be improved with further work on understanding the detector. Systematics can be also reduced by an improved resolution function or by a less efficient algorithm that trades statistical error for a better controlled resolution behavior. We project that an asymptotic systematic error of 0.010 can be achieved.

- **Signal dilutions:** This is presently evaluated by taking the difference between the B_{flav} and charmonium dilutions in Monte Carlo. In the future, we will be able to select the B_{flav} modes that are closest to the Charmonium sample (for instance just using $J/\psi\,K^*$) and thus reduce the error to about 0.010. Also, this source of error is not relevant for the lepton-tagged sample.

- **Non-K^0_L background:** At present, the CP-content of the background is varied over the range ± 1, which is very conservative. With higher statistics, we can measure this from the sidebands. We will also have a better knowledge of the charmonium modes that may be contributing to this background.

Sample	$N_{\rm sig}$	Statistical error on $\sin 2\beta$				
	$J/\psi\, K^0_S$	$J/\psi\, K^0_S$	$\eta_{CP}=-1$	All	$\eta_{CP}=-1$ Lepton	$\eta_{CP}=-1$ Kaon I
$81\,\text{fb}^{-1}$	940	0.084	0.074	0.067	0.113	0.119
$0.5\,\text{ab}^{-1}$	2,300	0.034	0.030	0.027	0.052	0.054
$2.0\,\text{ab}^{-1}$	4,700	0.017	0.015	0.013	0.026	0.027
$10.0\,\text{ab}^{-1}$	10,400	0.008	0.007	0.006	0.012	0.012
$50.0\,\text{ab}^{-1}$	23,400	0.003	0.003	0.003	0.005	0.005

Table 11: Projections of measurement errors on sin2β from $b \to c\bar{c}s$ modes. Signal yields are for tagged events.

Component	$81\,\text{fb}^{-1}$	$0.5\,\text{ab}^{-1}$	$2.0\,\text{ab}^{-1}$	$10.0\,\text{ab}^{-1}$	leptons
Δt	0.017	0.010	0.010	0.010	0.005
Dilutions	0.012	0.010	0.010	0.010	-
Non-K^0_L background	0.017	0.007	0.003	0.002	0.001
K^0_L Background	0.015	0.006	0.005	0.005	-
MC correction	0.010	0.004	0.002	0.001	0.003
DCSD	0.008	0.007	0.006	0.005	-
τ_B, Δm_d	0.005	0.002	0.002	0.002	0.002
Total Sys	0.034	0.019	0.017	0.016	0.006
Stat. (golden)	0.067	0.027	0.013	0.006	0.005

Table 12: Projections of systematic errors for the sin2β measurements. The last column refers to the lepton-tagged category alone, assuming an integrated luminosity of $50.0\,\text{ab}^{-1}$.

- ***J/ψ* K^0_L background:** The largest $J/\psi\, K^0_L$ systematic errors are actually statistical in nature (for example the signal fraction) and so this will improve as the sample grows. The analysis is intrinsically more complex than $J/\psi\, K^0_S$, so systematic errors will remain due to assumptions and measurements related to the large backgrounds. We assume that it will not be possible to improve the systematic error from this source below 0.005.

- **MC correction:** This contribution depends mostly on MC statistics and so scales nearly as $1/\sqrt{N}$.

- **DCSD decays:** This contribution is mostly due to ignoring the presence of doubly-CKM-suppressed transitions on the tag side of the events. Only modest improvement can be expected, given uncertainties in decay rates and phases. Eventually it may be possible to fit for the DCSD parameters and thereby reduce this error further.

- ***τ_B*, *Δm_d*:** The measurement of Δm_d will be systematics limited well before $\sin 2\beta$. Like $\sin 2\beta$, the systematic errors on Δm_d have statistical components and therefore

will continue to improve at least another factor of two.

We conclude that the sin2β measurement in charmonium modes will not be statistically limited until sample sizes in the range of 5–10 ab^{-1}. Even then, refinement of the *CP* sample and tagging methods will allow better tagging purity and Δt resolution, which would lead to further improvement in the measurement errors. For a sample of 2 ab^{-1}, the error on sin2β will be reduced to about 2.1% in total. The upgrades under consideration might lead to a further relative improvement of 3–5% for better Δt resolution and 0–5% for new tagging algorithms, as discussed in Sections 5.2 and 5.3.

6.1.2 Other modes

Sample	D^*D^*		$J/\psi\pi^0$		ϕK^0_S		$\eta' K^0_S$	
	N	$\sigma_{\sin2\beta}$	N	$\sigma_{\sin2\beta}$	N	$\sigma_{\sin2\beta}$	N	$\sigma_{\sin2\beta}$
82 fb^{-1}	93	0.29	40	0.49	40	0.51	109	0.34
0.5 ab^{-1}	570	0.12	245	0.20	245	0.21	665	0.14
2.0 ab^{-1}	2,300	0.06	1,000	0.10	1,000	0.10	2,700	0.07
10.0 ab^{-1}	11,300	0.03	4,900	0.04	4,900	0.05	13,000	0.03
50.0 ab^{-1}	57,000	0.01	24,000	0.02	24,000	0.02	66,000	0.01

Table 13: Projections of measurement errors on sin2β from $b \to c\bar{c}d$, $s\bar{s}s$, and $d\bar{d}s$ modes. Signal yields are for tagged events.

CP asymmetries in a variety of other modes are sensitive to sin2β in the Standard Model, but also probe whether direct *CP* violation due to competing diagrams is present or whether new physics contributes to Penguin amplitudes. These include $b \to c\bar{c}d$ modes such as $D^{(*)}D^{(*)}$ and $J/\psi\pi^0$, and $b \to s\bar{s}s$ or $b \to d\bar{d}s$ modes, such as ϕK^0_S or $\eta^{(\prime)}K^0_S$. *CP* asymmetries have been studied in these channels with the present data sample [9, 10, 11, 12]. Extrapolations of the number of tagged signal events and the corresponding measurement errors on the amplitude of the sine coefficient in the time-dependent asymmetries are provided in Table 13 for higher luminosities. At sample sizes of 0.5 ab^{-1}, the measurement errors for sin2β from these modes will be 12–20%. If we are able to accumulate samples as large as 2 ab^{-1}, where the errors are reduced to the 6–10% level, there is some chance of discriminating new sources of *CP* violation, although clearly much larger samples would be required for a definitive study.

6.2 Measuring $\sin 2\alpha$ with the decays $B^0 \to \pi^+\pi^-$

6.2.1 Projections for the measurement of α_{eff}

We have used our recently completed measurement of sin2α_{eff} as the basis for extrapolation to future data samples. The projected statistical and systematic errors are shown in Table 14.

Studies of the impact of improved Δt resolution have been undertaken with toy MC models of the existing measurement. A factor of two decrease in Δt resolution leads to

Sample	$N_{\rm sig}$	$S_{\pi\pi}$	$C_{\pi\pi}$
$81\,{\rm fb}^{-1}$	160	0.34 (0.05)	0.25 (0.04)
$0.5\,{\rm ab}^{-1}$	1,000	0.12 (0.03)	0.10 (0.03)
$2.0\,{\rm ab}^{-1}$	4,000	0.06 (0.03)	0.05 (0.03)
$10.0\,{\rm ab}^{-1}$	20,000	0.03 (0.03)	0.02 (0.03)

Table 14: Projections of measurement (systematic) errors on $\sin 2\alpha_{eff}$ from the mode $B^0 \to \pi^+\pi^-$.

a 15% reduction in the error $\sigma(S_{\pi\pi})$, which would be equivalent to a 30% increase in accumulated luminosity. No improvement in the error $\sigma(C_{\pi\pi})$ is seen. Recalling the study of the impact of upgrades on Δt resolution that are summarized in Table 10, these results for $\sigma(S_{\pi\pi})$ would be reduced to just a few percent in the any of the SVT upgrades under consideration.

6.2.2 Removing penguin contribution via isospin relations

Unlike the measurement of $\sin 2\beta$ in $B^0 \to J/\psi\, K^0_S$ and related channels the measurement of α in $Bz \to \pi^+\pi^-$ is beset by complications from penguin diagrams with weak phases that differ from those of the tree diagrams. The way around this was given by Gronau and London [13], which exploits the fact that penguin diagrams contribute only to $\Delta I = 1/2$ processes and an isospin analysis can therefore isolate the tree contribution.

The plan of attack is to measure $\sin 2\alpha_{eff}$ from the time dependence of $B^0 \to \pi^+\pi^-$ and $\overline{B}^0 \to \pi^+\pi^-$. The correction that allows one to convert $2\alpha_{eff}$ into the 2α is indicated by κ. The angle κ is found by determining two separate isospin triangles, one from B^0 decays and one from $\overline{B}^0$. The triangles are determined by the amplitude relation

$$\frac{\mathcal{A}^{+-}}{\sqrt{2}} + \mathcal{A}^{00} = \mathcal{A}^{+0} \tag{2}$$

so that the three sides are $\mathcal{B}(B^0 \to \pi^+\pi^-)/\sqrt{2}$, $\mathcal{B}(B^0 \to \pi^0\pi^0)$, and $\mathcal{B}(B^- \to \pi^-\pi^0)$, and similarly for $\overline{B}^0$. The branching fractions for the two decays $B^\pm \to \pi^\pm\pi^0$ must be equal. This follows because the final state cannot be $I = 1$ by Bose symmetry and thus is $I = 2$. On the other hand the penguin contribution is a $\Delta I = 1/2$ interaction and cannot change the $I = 1/2$ final state into an $I = 2$ final state. With only tree contributions, there cannot be direct *CP* violation for this process. These isospin relations are as illustrated in Fig. 13.

The angle κ is an angle between the B^0 and $\overline{B}^0$ triangles. Unfortunately there is an ambiguity in the orientation of the two triangles. Each of them can be "up" or "down," giving four possibilities and introducing a four-fold ambiguity in κ.

The real challenge in this suite of measurements is finding separately the B^0 and $\overline{B}^0$ branching fractions into $\pi^0\pi^0$. These branching fractions are color suppressed, that is, there is no diagram where the virtual W turn directly into an observed final particle. The current *BABAR* result is an upper limit of 3.6×10^{-6} for the average of the B^0 and $\overline{B}^0$

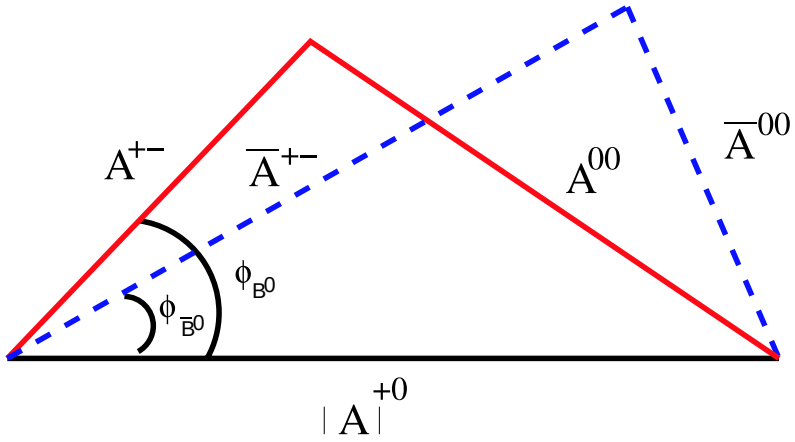

Figure 13: The Gronau-London construction for determining 2α. The phase $2\alpha_{eff}$ is found by measuring the time dependence of $B^0 \to \pi^+\pi^-$. The correction $2\alpha - 2\alpha_{eff}$ is given by $\pm(\phi \pm \phi')$. There is a four-fold ambiguity because there is no way to know *a priori* the orientation of the two triangles.

branching fractions into $\pi^0\pi^0$, while the other branching fractions are measured to be

$$\begin{aligned} \mathcal{B}(B^+ \to \pi^+\pi^0) &= 5.5^{+1.0}_{-0.9} \pm 0.6 \times 10^{-6} \text{ (with 81 fb}^{-1} \text{ [14])} \\ \mathcal{B}(B \to \pi^+\pi^-) &= 4.7 \pm 0.6 \pm 0.2 \times 10^{-6} \text{ (with 81 fb}^{-1} \text{ [15])}. \end{aligned} \tag{3}$$

The backgrounds in these channels have been estimated by Roodman [16] in studies for a 10^{36} machine. They are given as effective branching fractions.

$$\begin{aligned} \sigma(\mathcal{B}(B^0 \to \pi^+\pi^0)) &= 2.1\sqrt{22.0/\int dt\mathcal{L}} \\ \sigma(\mathcal{B}(B^0 \to \pi^+\pi^-)) &= 1.2\sqrt{22.0/\int dt\mathcal{L}} \\ \sigma(A_{cos}) &= 0.5\sqrt{33.0/\int dt\mathcal{L}} \end{aligned} \tag{4}$$

For the critical $\pi^0\pi^0$ measurement, tagging is essential. Not only do we need to know the efficiency and wrong-tag probability for each tagging category, we also need to know the background, which will vary from category to category. The values we have used are shown in Table 15.

We have considered four distinct toy Monte Carlo models, defined by different assumptions for branching fractions and backgrounds. Everywhere, we have used Roodman's estimate for the reconstruction efficiency for the $\pi^0\pi^0$ final state: $\epsilon_{reco} = 0.18$. To establish a limiting case, in one model (C) we neglect all backgrounds. In the other models,

Category	ϵ	D	$\mathcal{B}$
Lepton	0.09	0.93	2.0
Kaon I	0.16	0.82	4.0
Kaon II	0.20	0.56	5.0
Inclusive	0.20	0.41	6.0

Table 15: Assumed tagging performance, based on the Moriond Tagger. The final column gives the background as an effective branching fraction, in units of 10^{-6}.

the backgrounds are given by Table 15. The branching fractions for the four models are given in Table 16. To optimize the performance, we have used both tagged and untagged data for $B^0 \to \pi^0\pi^0$ and $\overline{B}^0 \to \pi^0\pi^0$. Whenever the Monte Carlo experiment violated the triangular inequality, we have taken ϕ_{B^0} (or $\phi_{\overline{B}^0}$) to be zero.

The results of the MC studies are shown in Table 17 and in Figs.14-17. The general conclusion is that a decent measurement is out of reach with an integrated luminosity of $0.5\,\mathrm{ab}^{-1}$. Indeed, even $2\,\mathrm{ab}^{-1}$ is inadequate. A reasonable criterion would be that we need enough integrated luminosity that if the Standard Model breaks down by having α not fit the unitarity triangle, we should be able to demonstrate this by three sigma. Of course, we can succeed only if the breakdown is large enough.

According to Table 17, which does not take into account the four-fold ambiguity, it appears that a three-sigma effect could be seen only for the most fortuitous cases with an integrated luminosity of $2\,\mathrm{ab}^{-1}$, except perhaps in the idealized case of no background. The situation is still more challenging when the ambiguities are considered, as shown in the Figures. The way that the ambiguities enter depends on the shapes of the triangles, but the example here is probably representative.

In conclusion, the small branching fraction into $\pi^0\pi^0$ and the need to measure this branching fraction separately for B^0 and $\overline{B}^0$ will make the measurement of α in the $\pi\pi$ channel a severe challenge throughout the *BABAR* experiment, even under the best of circumstances.

Channel	Model A	Model B	Model C	Model D
$B^\pm \to \pi^\pm\pi^0$	4.1	4.1	4.1	4.1
$B^0 \to \pi^+\pi^-$	4.7	4.7	4.7	4.7
$\overline{B}^0 \to \pi^+\pi^-$	4.7	4.7	4.7	4.7
$B^0 \to \pi^0\pi^0$	2.5	1.5	2.5	0.6
$\overline{B}^0 \to \pi^0\pi^0$	1.5	0.5	1.5	0.4

Table 16: Branching fractions assumed for the four models A, B, C, and D, in units of 10^{-6}.

$\int dt\mathcal{L}$ [ab^{-1}]	κ	ϕ_{B^0}	$\phi_{\overline{B}^0}$	$\mathcal{B}$	$\overline{\mathcal{B}}$
Model A: $\mathcal{B}(B^0, \overline{B}^0 \to \pi^0\pi^0) = 2.5, 1.5 \times 10^{-6}$					
10.	0.075	0.037	0.046	0.173	0.167
5.	0.108	0.053	0.067	0.245	0.237
2.	0.177	0.086	0.112	0.391	0.378
1.	0.269	0.126	0.173	0.561	0.545
0.5	0.409	0.201	0.254	0.820	0.804
Model B: $\mathcal{B}(B^0, \overline{B}^0 \to \pi^0\pi^0) = 1.5, 0.5 \times 10^{-6}$					
10.	0.132	0.043	0.100	0.157	0.150
5.	0.181	0.062	0.136	0.222	0.213
2.	0.258	0.104	0.180	0.355	0.341
1.	0.339	0.162	0.214	0.511	0.494
0.5	0.452	0.248	0.253	0.757	0.744
Model C: $\mathcal{B}(B^0, \overline{B}^0 \to \pi^0\pi^0) = 2.5, 1.5 \times 10^{-6}$, no bkgd					
10.	0.045	0.024	0.028	0.103	0.097
5.	0.064	0.034	0.041	0.147	0.138
2.	0.106	0.054	0.067	0.237	0.225
1.	0.164	0.081	0.106	0.351	0.339
0.5	0.286	0.140	0.183	0.711	0.809
Model D: $\mathcal{B}(B^0, \overline{B}^0 \to \pi^0\pi^0) = 0.6, 0.4 \times 10^{-6}$					
10.	0.175	0.081	0.112	0.145	0.143
5.	0.235	0.122	0.140	0.206	0.203
2.	0.316	0.177	0.173	0.330	0.326
1.	0.372	0.213	0.205	0.478	0.473
0.5	0.436	0.253	0.242	0.717	0.723

Table 17: The rms spreads on κ (the correction to $2\alpha_{eff}$), ϕ_{B^0} (the relevant angle in the B^0 triangle), $\phi_{\overline{B}^0}$, $\mathcal{B}$ (the branching fraction for $B^0 \to \pi^0\pi^0$), $\overline{\mathcal{B}}$. The four-fold discrete ambiguity has been ignored for this result, which represents the spread for one choice of triangle orientation.

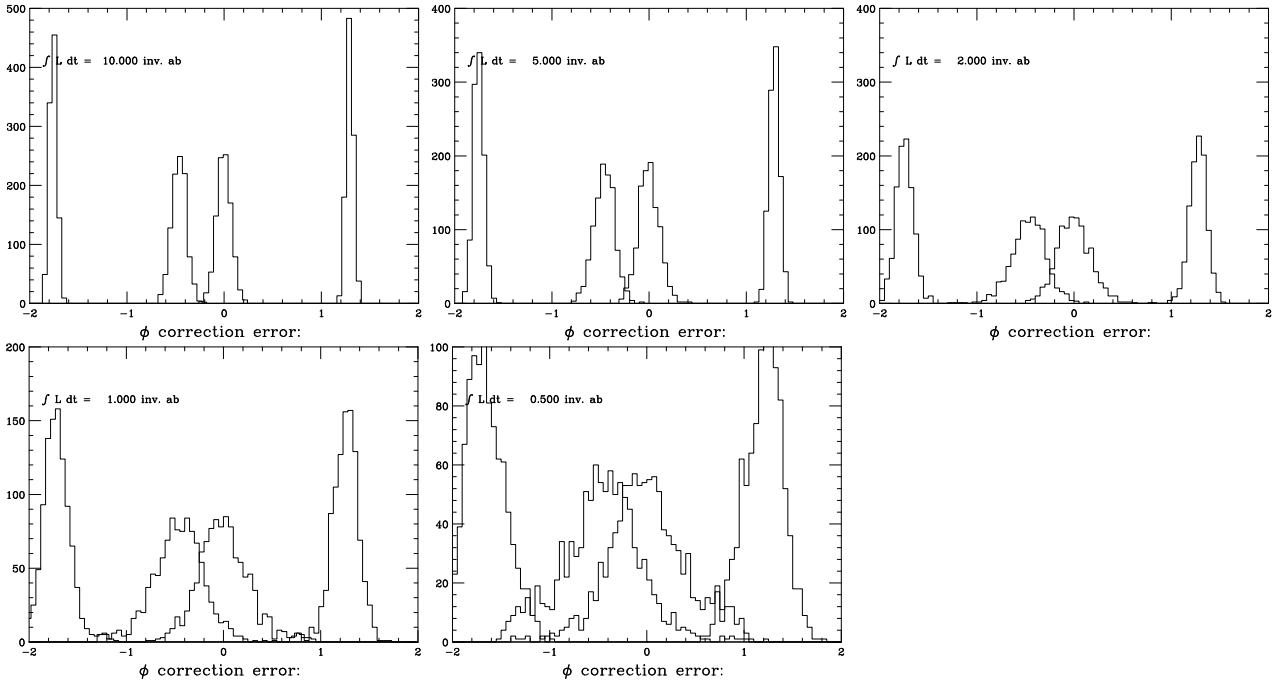

Figure 14: Results for Model A

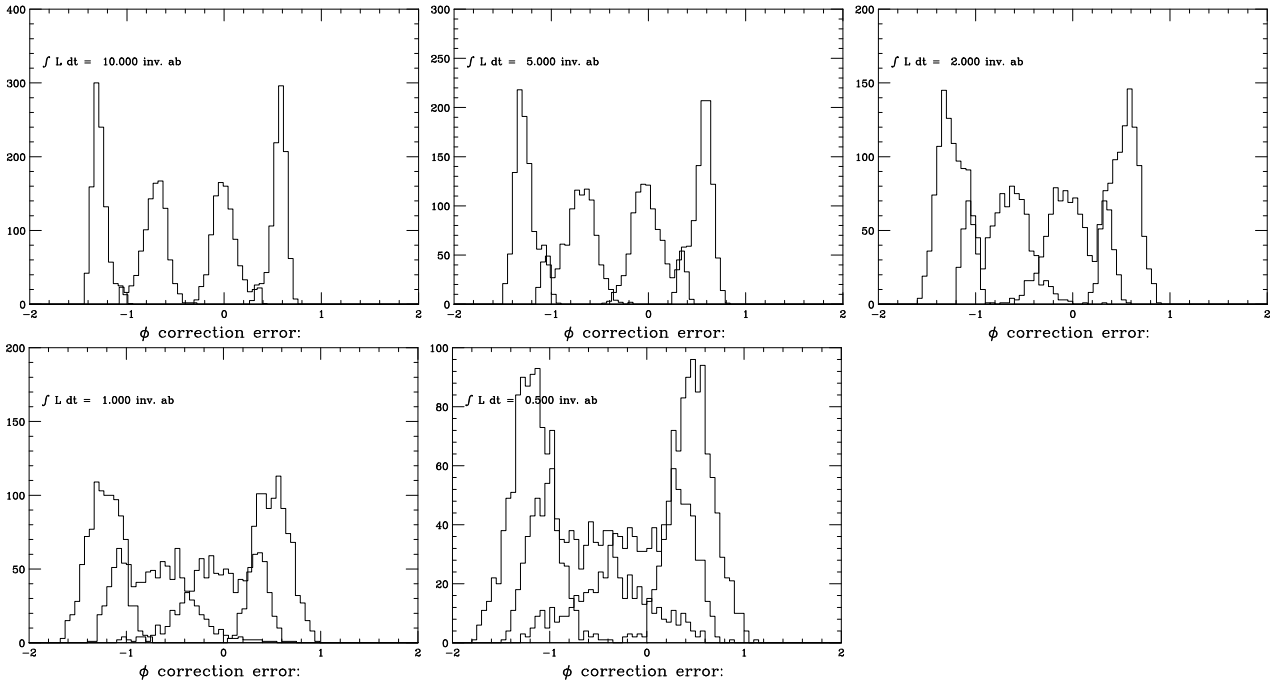

Figure 15: Results for Model B

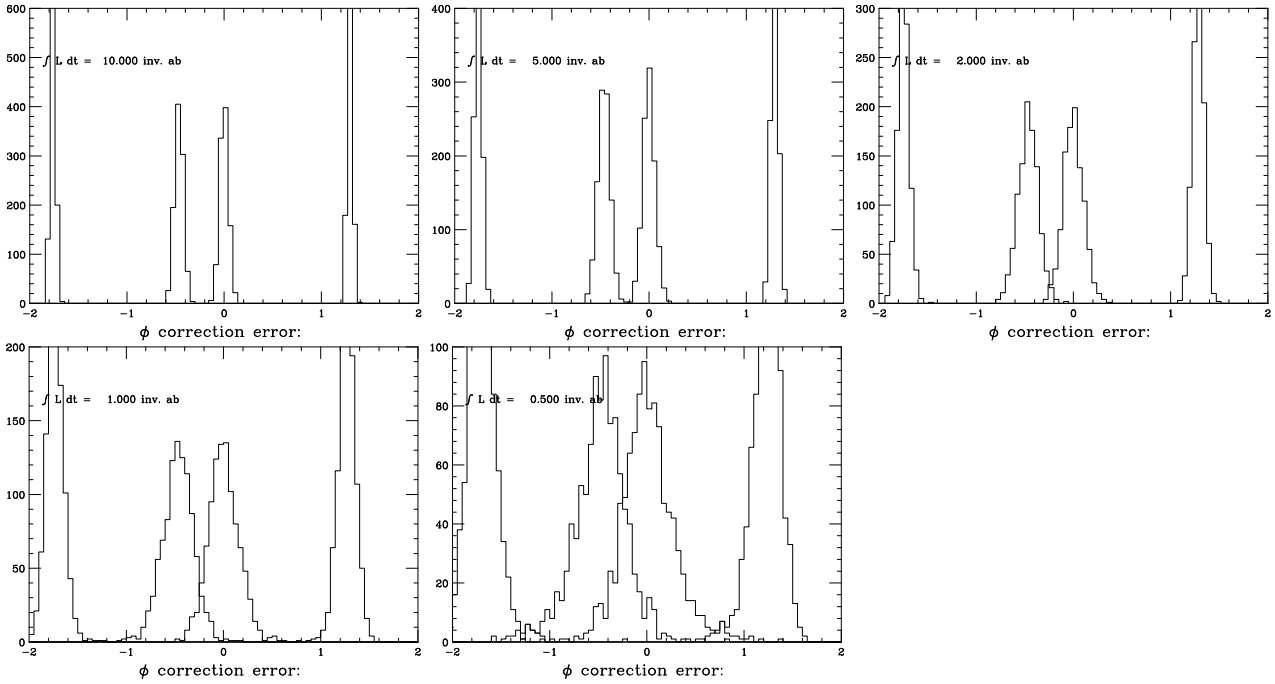

Figure 16: Results for Model C

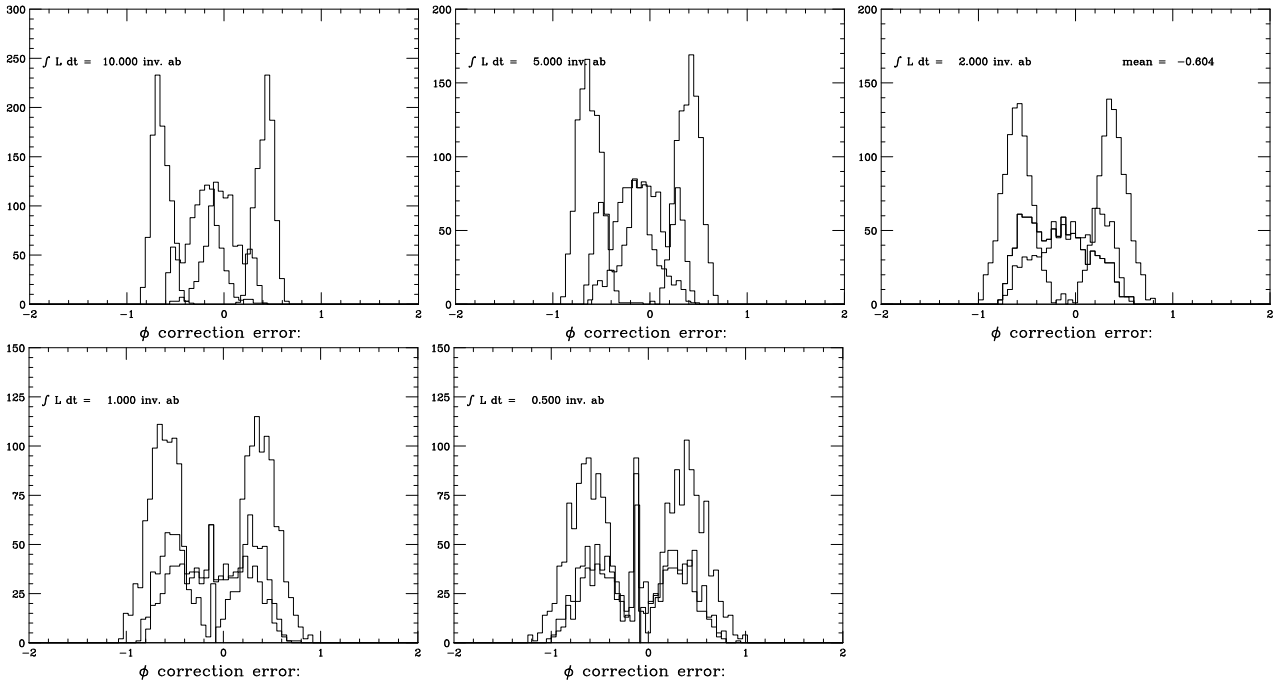

Figure 17: Results for Model D

6.2.3 Using the Grossman-Quinn bound to constrain penguin pollution

One constraint, known as the Grossman-Quinn bound, on the contribution of penguin pollution to $B \to \pi\pi$ decays can be obtained from the ratio of the *CP* averaged branching fractions, $\sin^2(\delta\alpha) < \mathcal{B}(B \to \pi^0\pi^0)/\mathcal{B}(B \to \pi^+\pi^0)$, where $\delta\alpha = \alpha_{eff} - \alpha$ [17]. Other bounds with better coverage can also be found in the literature [18], but these require more theoretical input. The power of a bound on $|\delta\alpha|$ comes into its own when $\mathcal{B}(B \to \pi^0\pi^0)$ is small. The current experimental status from *BABAR* is that we have a central value of 1.6×10^{-6} for the $B \to \pi^0\pi^0$ branching fraction, which corresponds to $|\delta\alpha| < 51^\circ$ given our ICHEP 2002 result for $\mathcal{B}(B \to \pi^+\pi^0)$. Figure 18 shows the variation of the 90% upper limit as a function of $\mathcal{B}(B \to \pi^0\pi^0)$. The lines drawn on the plot are for the perfect result (infinite luminosity) and for results obtained by assuming that the error on the branching fraction scales linearly from $\mathcal{B}(B \to \pi^0\pi^0) = 2.0 \times 10^{-6}$ to other luminosities. Toy Monte Carlo results are plotted for different branching fractions assuming luminosities from 0.5–10.0 ab^{-1}; these show that the assumed scaling is invalid for very small $B \to \pi^0\pi^0$ branching fractions (*i.e.*, $< 0.5 \times 10^{-6}$).

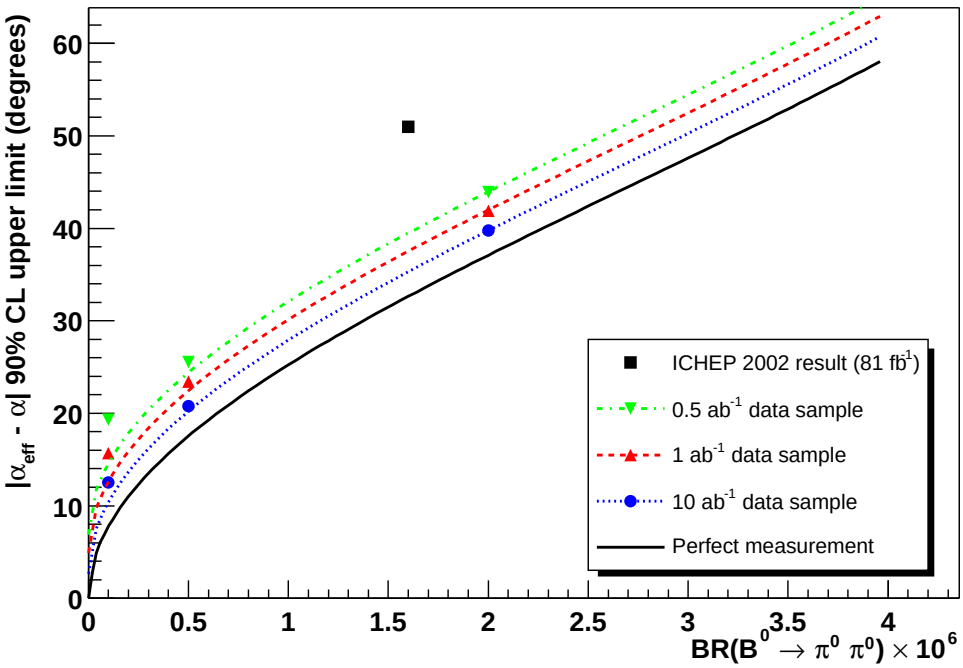

Figure 18: The upper limit on $|\delta\alpha|$ as a function of $\mathcal{B}(B \to \pi^0\pi^0)$ for different luminosities.

In the limit of large data samples one could obtain at best $\delta\alpha < 39^\circ$ assuming a central value of $\mathcal{B}(B \to \pi^0\pi^0) = 2 \times 10^{-6}$, which is only slightly better than what we have achieved thus far. For an assumed signal branching fraction of 0.5×10^{-6} we could obtain at best $|\delta\alpha| < 19^\circ$. It is clear from this that the Grossman-Quinn bound on $\sin^2(\delta\alpha)$ will not yield a precision measurement of $\delta\alpha$ unless one has a true $\mathcal{B}(B \to \pi^0\pi^0)$ significantly less than the lower end of theoretical expectations. There is approximately an 8–10° improvement

in the measurement when increasing the luminosity from 0.5 to 10.0 ab^{-1}. This is true for all of the scenarios tested. There is little improvement on the obtained bound, once the data sample exceeds O(2 ab^{-1}). Furthermore, if one compares the upper limits obtained from the different scenarios for the "best" and "worst" cases with respect to observation of $B \to \pi^0\pi^0$, there is very little difference on the upper limit on $|\delta\alpha|$. From this we conclude that one should not hope to gain a much better upper limit on the bound from minor improvements in the $B \to \pi^0\pi^0$ analysis.

If one improves the $B \to \pi^0\pi^0$ signal tails in the δE distribution then there is very little change in the above results. This can be understood from the fact that δE actually brings very little to the $B \to \pi^0\pi^0$ analysis given the signal shape and dominance of continuum background in the data. If the resolution of the calorimeter were to be halved, then one could benefit from a slightly smaller error on the $\pi^0\pi^0$ yield ($\sim 10\%$). This arises because in a better calorimeter ΔE is more pronounced and better at discriminating between signal and continuum than the current design. The bound placed on $|\delta\alpha|$ with a better calorimeter is only marginally improved over that attainable with the current design.

In summary, one should expect to gain most of the information available from this method within the lifetime of the first-generation B Factories (assuming that this corresponds to a total data sample in the range 1–2 ab^{-1}). The limiting factor is the true value of the branching fraction for $B \to \pi^0\pi^0$, which remains unknown with a highest statistics upper limit available of $< 3.6 \times 10^{-6}$ where theoretical predictions lie in the range $0.5\text{–}4.7 \times 10^{-6}$ [19]. Further details of this discussion can be found in Ref. [20].

6.3 Measuring γ with the decays $B^- \to D_{CP}K^-$

This section describes a study of the feasibility of measuring the CKM angle γ through the reconstruction of the decays $B^\pm \to D^0K^\pm$, where the D^0 meson is selected in the $CP = +1$ and $CP = -1$ eigenstates in a method based on the original 1991 proposal of Gronau-London-Wyler [21].

6.3.1 Method of extraction of $\sin^2\gamma$

Consider the decays $B^\pm \to D_1^0(D_2^0)K^\pm$, where $D_1^0(D_2^0) \equiv (D^0 + (-)\overline{D}^0)/\sqrt{2}$ is a *CP*-even (odd) state. The state $D_{1,2}^0$ can be identified by its *CP*-even (odd) decay products, neglecting *CP* violation in D decays. For example, the channels K^+K^- and $\pi^+\pi^-$ must come from a D_1^0, while the channel $K_S^0\pi^0$ identifies a D_2^0.

The amplitudes for the decays $B^\pm \to D_1^0K^\pm$, $B^\pm \to D^0K^\pm$ and $B^\pm \to \overline{D}^0K^\pm$ are constrained by the relation

$$\sqrt{2}A(B^+ \to D_1^0K^+) = A(B^+ \to D^0K^+) + A(B^+ \to \overline{D}^0K^+), \quad (5)$$

$$\sqrt{2}A(B^- \to D_1^0K^-) = A(B^- \to D^0K^-) + A(B^- \to \overline{D}^0K^-). \quad (6)$$

where the decay $B^+ \to \overline{D}^0K^+$ is dominated by the tree process $\overline{b} \to u\overline{c}s \propto V_{cb}^*V_{us}$ ($\propto \lambda^3$, color-allowed), while the decay $B^+ \to D^0K^+$ results from the tree process $\overline{b} \to \overline{u}c\overline{s} \propto V_{ub}^*V_{cs}$ ($\propto \lambda^3$, color-suppressed).

In the standard parameterization of the CKM matrix, only the elements V_{td} and V_{ub} have a phase different from zero. Thus:

$$arg(V_{cb}^* V_{us}) = 0 \tag{7}$$

$$arg(V_{ub}^* V_{cs}) = arg(V_{ub}^*) = arg(\overbrace{-\frac{V_{ud}}{V_{cd}V_{cb}}}^{real}\ V_{ub}^*) \equiv \gamma \tag{8}$$

Based on the results in Eq. (7) and (8), the B^+ decay amplitudes can be written as:

$$A(B^+ \to \overline{D}^0 K^+) = |\overline{A}|e^{i\overline{\delta}} \tag{9}$$

$$A(B^+ \to D^0 K^+) = |A|e^{i\delta}e^{i\gamma} \tag{10}$$

Likewise, the B^- decay amplitudes take the form:

$$A(B^- \to D^0 K^-) = |\overline{A}|e^{i\overline{\delta}} \tag{11}$$

$$A(B^- \to \overline{D}^0 K^-) = |A|e^{i\delta}e^{-i\gamma} \tag{12}$$

Defining the decay amplitudes of the $B^\pm \to D^0/\overline{D}^0 K^\pm$ as in equations (9–12), one easily finds:

$$\Gamma(B^+ \to \overline{D}^0 K^+) = \Gamma(B^- \to D^0 K^-) = |\overline{A}|^2 \tag{13}$$

$$\Gamma(B^+ \to D^0 K^+) = \Gamma(B^- \to \overline{D}^0 K^-) = |A|^2 \tag{14}$$

$$\Gamma(B^\pm \to D_1^0 K^\pm) = \tfrac{1}{2}[|\overline{A}|^2 + |A|^2 + 2|\overline{A}||A|\cos(\Delta\delta \pm \gamma)] \tag{15}$$

$$\Gamma(B^\pm \to D_2^0 K^\pm) = \tfrac{1}{2}[|\overline{A}|^2 + |A|^2 - 2|\overline{A}||A|\cos(\Delta\delta \pm \gamma)] \tag{16}$$

where $\Delta\delta \equiv \delta - \overline{\delta}$ is the strong phase difference. If we introduce the ratio $r \equiv |A(B^- \to \overline{D}^0 K^-)|/|A(B^- \to D^0 K^-)|$, the *CP* asymmetries for decays into $D_1^0 K^\pm$ and $D_2^0 K^\pm$, normalized by the rate into the D meson flavor state,

$$A_i \equiv \frac{\Gamma(B^- \to D_i^0 K^-) - \Gamma(B^+ \to D_i^0 K^+)}{\Gamma(B^- \to \overline{D}^0 K^-) + \Gamma(B^+ \to D^0 K^+)}, \quad i = 1, 2, \tag{17}$$

are equal in magnitude and have opposite signs:

$$A_1 \;=\; +r\,\sin\Delta\delta\,\sin\gamma \tag{18}$$

$$A_2 \;=\; -r\,\sin\Delta\delta\,\sin\gamma \tag{19}$$

Any observation of A_1 or A_2 different from zero would be the proof of direct *CP* violation in the B system. A_1 and A_2 yield a combined asymmetry

$$A_{CP} \equiv A_1 - A_2 = 2r\sin\Delta\delta\sin\gamma. \tag{20}$$

It is convenient to define two charge-averaged ratios for the two *CP* eigenstates

$$R_i \equiv \frac{2[\Gamma(B^+ \to D_i^0 K^+) + \Gamma(B^- \to D_i^0 K^-)]}{\Gamma(B^+ \to \overline{D}^0 K^+) + \Gamma(B^- \to D^0 K^-)}, \quad i = 1, 2, \tag{21}$$

for which we find

$$R_{1,2} = 1 + r^2 \pm 2r \cos\Delta\delta \cos\gamma. \tag{22}$$

The factor 2 in the definition of $R_{1,2}$ is used to approximately normalize these ratios to one (r is expected to be significantly smaller than one). The relations (20) and (22) represent a system of 3 equations in the 3 unknowns (r, $\Delta\delta$, γ):

$$A_{CP} = 2r \sin\Delta\delta \sin\gamma\,, \tag{23}$$
$$R_1 = 1 + r^2 + 2r \cos\Delta\delta \cos\gamma\,, \tag{24}$$
$$R_2 = 1 + r^2 - 2r \cos\Delta\delta \cos\gamma\,. \tag{25}$$

After introducing the quantities

$$\alpha^2 \equiv \frac{(R_1 - R_2)^2}{8(R_1 + R_2 - 2)} \tag{26}$$
$$\beta^2 \equiv \frac{A_{CP}^2}{2(R_1 + R_2 - 2)} \tag{27}$$

the solutions for $\sin^2\gamma$ are found:

$$\sin^2\gamma \;=\; \frac{1 + \beta^2 - \alpha^2}{2} \pm \sqrt{\left(\frac{1 + \beta^2 - \alpha^2}{2}\right)^2 - \beta^2}\,. \tag{28}$$

6.3.2 Evaluation of the precision in the $\sin^2\gamma$ extraction

Eq. (28) gives $\sin^2\gamma$ as a function of the measurable quantities A_{CP}, R_1 and R_2. The presence of two solutions is a consequence of the 8-fold discrete ambiguity in the extraction of γ (and hence a two-fold ambiguity in $\sin^2\gamma$) intrinsic in this method. A_{CP}, R_1 and R_2 are evaluated through the direct measurement[1] of

$$\Gamma_{1-} \equiv \frac{\Gamma(B^- \to D_1 K^-)}{\Gamma(B^- \to D^0 K^-)} = \frac{1 + r^2}{2} + r\cos(\Delta\delta - \gamma) \tag{29}$$
$$\Gamma_{1+} \equiv \frac{\Gamma(B^+ \to D_1 K^+)}{\Gamma(B^- \to D^0 K^-)} = \frac{1 + r^2}{2} + r\cos(\Delta\delta + \gamma) \tag{30}$$
$$\Gamma_{2-} \equiv \frac{\Gamma(B^- \to D_2 K^-)}{\Gamma(B^- \to D^0 K^-)} = \frac{1 + r^2}{2} - r\cos(\Delta\delta - \gamma) \tag{31}$$
$$\Gamma_{2+} \equiv \frac{\Gamma(B^+ \to D_2 K^+)}{\Gamma(B^- \to D^0 K^-)} = \frac{1 + r^2}{2} - r\cos(\Delta\delta + \gamma) \tag{32}$$

R_1, R_2 and A_{CP} are simply related to $\Gamma_{i,\pm}$ through

$$R_1 = \Gamma_{1,-} + \Gamma_{1,+}\,, \tag{33}$$
$$R_2 = \Gamma_{2,-} + \Gamma_{2,+}\,, \tag{34}$$
$$A_{CP} = (\Gamma_{1,-} - \Gamma_{1,+} - \Gamma_{2,-} + \Gamma_{2,+})/2\,. \tag{35}$$

[1]Note that measurements of the *absolute* branching fractions for $B^\pm \to D^0_{1,2} K^\pm$ are not required, only the branching ratios normalized by $\Gamma(B^- \to D^0 K^-)$.

Based on a current *BABAR* analysis of $B \to D^0 K$ [22, 23] with a data sample equivalent to an integrated luminosity of $75\,\mathrm{fb}^{-1}$, we obtain the following width results

$$\Gamma_{1,+} = 0.72 \pm 0.26 \pm 0.02\,, \tag{36}$$

$$\Gamma_{1,-} = 1.02 \pm 0.29 \pm 0.02\,, \tag{37}$$

which then can be used to project the experimental uncertainties to larger samples. We parameterize the uncertainty as

$$\Delta\Gamma_{i,\pm} = \alpha_i \sqrt{\Gamma_{i,\pm}} \sqrt{\frac{100 fb^{-1}}{\int L dt}} \oplus \sigma_i \tag{38}$$

where the coefficient α_i is determined experimentally and σ_i takes into account any systematic uncertainty that is not reduceable with increasing statistics. The evaluation of the coefficient α_1 is based on the measurements in Eq. (36) and (37). We make the assumptions that we will be able to enlarge the $CP = +1$ sample by a factor of 1.5 by including other modes and the $CP = -1$ and $CP = +1$ samples will be comparable in size.

Four different scenarios are considered: a) actual detector performance; b) "perfect" apparatus performance; c) actual detector with the reconstruction of $B \to D^{*0} K$ and $B \to D^0 K^*$ decays; d) "perfect" apparatus performance with the reconstruction of $B \to D^{*0} K$ and $B \to D^0 K^*$ decays. We indicate with the label "perfect apparatus" the case where the errors on the yields are equal to the square root of the yields. A systematic uncertainty σ_i of 0.01 is assumed in all scenarios. The values of the coefficients α_i and σ_i are reported in Table 18.

Scenario	α_i	σ_i
$B \to D^0 K$, actual detector	0.208	0.01
$B \to D^0 K$, "perfect apparatus"	0.156	0.01
$B \to D^{(*)0} K^{(*)0}$, actual detector	0.177	0.01
$B \to D^{(*)0} K^{(*)0}$, "perfect apparatus"	0.133	0.01

Table 18: Value of coefficients that enter the parameterization of the $\Gamma_{i,\pm}$ uncertainties in Eq. (38).

The procedure to estimate the precision for $\sin^2\gamma$ with a given integrated luminosity is as follows. Fixed values of the *true* parameters (r, $\Delta\delta$, γ) are used to evaluate the corresponding values for the *true* $(\Gamma_{1-}, \Gamma_{1+}, \Gamma_{2-}, \Gamma_{2+})_{true}$ ratios based on the relations (29-32). In a set of 1000 toy experiments the *measured* values $(\Gamma_{1-}, \Gamma_{1+}, \Gamma_{2-}, \Gamma_{2+})_{meas}$ are generated from Gaussian distributions with means given by the true values $(\Gamma_{1-}, \Gamma_{1+}, \Gamma_{2-}, \Gamma_{2+})_{true}$ and widths given by Eq. (38). Simulated measurements for $(A_{CP}, R_1, R_2)_{meas}$ are derived from $(\Gamma_{1-}, \Gamma_{1+}, \Gamma_{2-}, \Gamma_{2+})_{meas}$ according to relations (33-35). Finally, the corresponding pair of results for $\sin^2\gamma$ (when the solutions are real) are derived from Eq. (28).

Several sets of experiments have been performed, with different values of $(r, \Delta\delta, \gamma)_{true}$, different integrated luminosities and different detector scenarios. The results are summarized in Table 19, where the mean and rms of the simulated $\sin^2\gamma_{meas}$ distributions

r_{true}	$\Delta\delta_{true}$	γ_{true}	scenario	$\int \mathcal{L}\, dt\, [\mathrm{ab}^{-1}]$	$\sin^2\gamma_{meas}$ mean	$\sin^2\gamma_{meas}$ rms
0.3	0°	60°	perfect app.	2.0	0.73	0.09
0.3	0°	60°	actual det.	2.0	0.72	0.13
0.3	0°	60°	perfect app.	0.5	0.70	0.21
0.3	0°	60°	actual det.	0.5	0.69	0.25
0.2	0°	60°	perfect app.	2.0	0.70	0.22
0.2	0°	60°	actual det.	2.0	0.73	0.25
0.2	0°	60°	perfect app.	0.5	0.77	0.29
0.2	0°	60°	actual det.	0.5	0.82	0.30
0.1	0°	60°	perfect app.	2.0	0.91	0.28
0.3	20°	60°	perfect app.	2.0	0.74	0.08
0.3	20°	60°	actual det.	2.0	0.74	0.10
0.2	20°	60°	perfect app.	2.0	0.77	0.14
0.2	20°	60°	actual det.	2.0	0.81	0.18

Table 19: Mean and rms of the distribution for $\sin^2\gamma_{meas}$, assuming different sets of input parameters and integrated luminosities.

r_{true}	$\Delta\delta_{true}$	γ_{true}	scenario	$\int \mathcal{L}\, dt\, [\mathrm{ab}^{-1}]$	A_{CP} mean	A_{CP} rms
0.2	30°	60°	actual det.	0.5	0.174	0.053
0.2	30°	60°	perfect app.	0.5	0.173	0.043
0.2	30°	60°	actual det.	2.0	0.174	0.031
0.2	30°	60°	perfect app.	2.0	0.173	0.023

Table 20: Mean and width of the distribution for the direct *CP* asymmetry A_{CP}, assuming different scenarios and integrated luminosities.

are reported for each set of conditions. The "perfect apparatus" and "actual detector" scenarios in Table 19 refer to the case in which the general $B \to D^{(*)0}K^{(*)0}$ decays are reconstructed.

The distributions of $\sin^2\gamma_{meas}$ for some representative sets of conditions and scenarios are shown in Fig. 19. Two different peaks are visible, corresponding to the two solutions for $\sin^2\gamma$ that are intrinsic in the GLW method (Eq. (28)): one is centered around $\sin^2\gamma_{true}$, the other around $\sin^2\Delta\delta_{true}$ ($\gamma \leftrightarrow \Delta\delta$ ambiguity). We find that the achievable precision for γ depends critically on the assumed value for the ratio r. If r is 0.1 or smaller, it will be very difficult to extract useful information on γ with this method, even for an integrated luminosity of a few ab^{-1} (see Figure 19, bottom plot). On the other hand, if $r \gtrsim 0.2$ the situation is more promising (see Table 20 and the three upper plots in Fig. 19). This follows from the fact that the GLW method is able to provide information on $\sin^2\gamma$ when the experimental errors are small enough to resolve r^2; hence the feasibility of this measurement depends quite sensitively on the actual value of r. It is expected that r

will be in the range (0.1-0.2), but there are no precise estimates at the moment. A lower limit can be given by the measurement of the direct *CP* asymmetry; from Eq. (20) it follows that $r > |A_{CP}/2|$. Table 20 summarizes the achievable precision on the direct *CP* asymmetry for different scenarios and integrated luminosities.

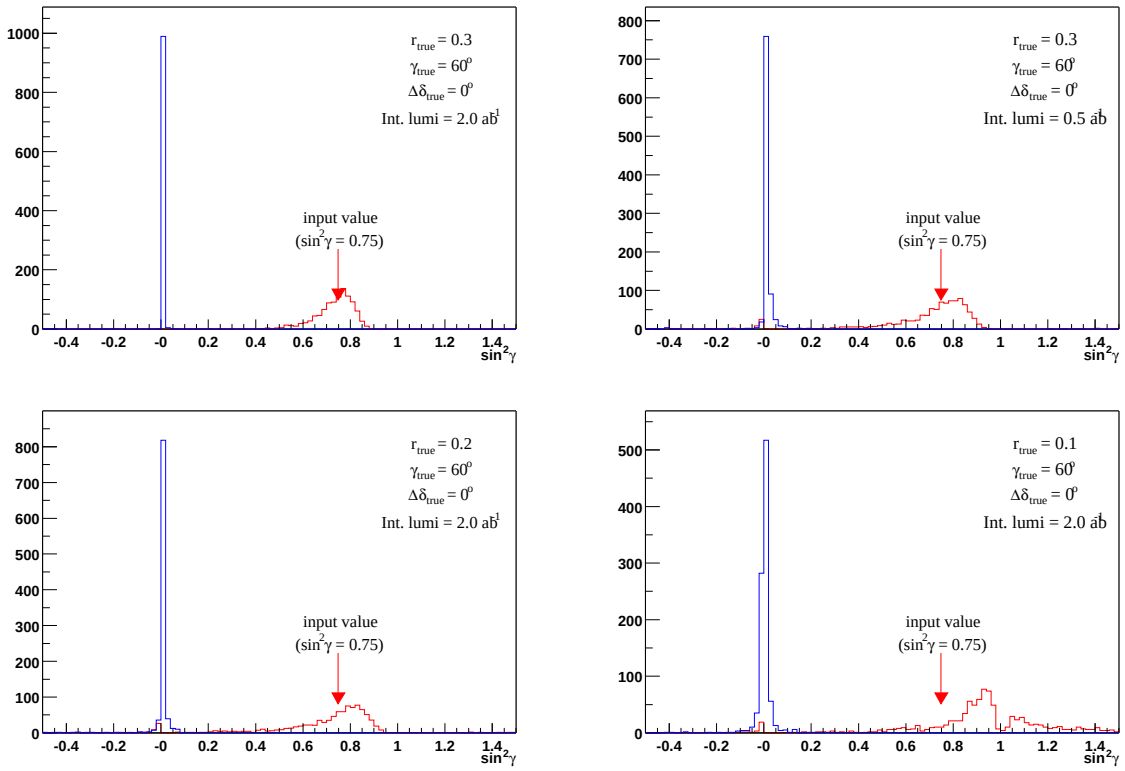

Figure 19: Distribution of $\sin^2\gamma$ measurements ("perfect apparatus" scenario) from a set of 1000 toy MC experiments. The input conditions are reported on each figure. The arrow indicates the true value of $\sin^2\gamma$ used in the toy MC.

6.4 Extraction of V_{ub}

The extraction of $|V_{ub}|$ is a challenge both for theory and experiment. Experimentally, the main problem is the separation of $b \to u\ell\nu$ decays from the dominant $b \to c\ell\nu$ decays. Selection criteria applied to achieve this separation generally make it difficult to translate the observed rate to the full decay rate. Theoretically, inclusive semi-leptonic rates can be calculated reliably at the parton level. However, meson decays processes depend on the b quark mass and its motion inside the B meson. Calculations of the decay rate in terms of $|V_{ub}|$ rely on operator product expansions (OPE) in inverse powers of the b quark mass and thus depend on the choice of renormalization scale and include non-perturbative contributions.

The large B sample collected with *BABAR* allows us to exploit a new technique for extracting $|V_{ub}|$, which is much cleaner than the previous attempts and therefore allows

smaller experimental and theoretical uncertainties. The new method involves the extraction of $|V_{ub}|$ from the invariant mass M_X of the hadronic system recoiling against the charged lepton and the neutrino in $B \to X_u \ell\nu$ transition. The ongoing analysis at *BABAR* [24] incorporates the following strategy:

- Fully reconstruct one B meson (2K B^+, 1K B^0/ fb^{-1}) in modes involving a $D^{(*)}$ meson [25];
- Require a lepton with $p^* > 1\,\mathrm{GeV}/c$;
- Reconstruct all the particles recoiling against the reconstructed B candidate and the lepton (the so called X system);
- Compute the event missing mass squared (M_ν^2) and require this to be consistent with 0;
- Apply a kinematic fit to improve resolution on the X system invariant mass, M_x;
- Require charge balance and the absence of any kaon (charged or neutral) on the recoil side of the event; and
- Use the spectrum of M_x to discriminate between $b \to u l\nu$ (signal) and $b \to c l\nu$ background events.

The signal events currently obtained with these requirements contributes a statistical error of about 7% to $|V_{ub}|$ in a $80\,\mathrm{fb}^{-1}$ data sample and the ratio of signal over background below $M_x < 1.55\,\mathrm{GeV}/c^2$ is almost two-to-one.

6.4.1 Sensitivity extrapolations

Scaling the present error based on Poisson statistics, the statistical error is expected to be 2.8%, 1.1% and 0.6% in 0.5, 3 and 10 ab^{-1} of accumulated data respectively.

The experimental systematic error is of the same order of magnitude and is dominated by the the knowledge of the $b \to c l\nu$ background. It is therefore expected to become smaller either with better understanding of the underlying physics (in particular the knowledge of the B and D decay rates) or by better background rejection. Since the low M_x tail of the background (which at generator level does not extend below $1.8\,\mathrm{GeV}/c^2$) is dominated by D decays into K_L^0 where the energy of the K_L^0 is underestimated and its mass neglected, better identification of the neutral hadrons would be highly beneficial for this measurement.

Theoretical errors are also about 8% and are dominated by the uncertainty on the fraction of $b \to u l\nu$ events above the M_x cut. This uncertainty is due to an incomplete knowledge of the dynamics of the b quark inside the B meson, and to the fact that the assumption of parton-meson duality is not exact. There are therefore three means to reduce these theoretical systematics:

- Choose the M_x cut in order to reduce the range of extrapolation. The optimal cut can be chosen each time minimizing the total error (as it is done in the current analysis) so that the statistical error will not actually scale with Poisson statistics;

- Understand b quark dynamics better, in particular by means of $b \to s\gamma$ events. There are suggested approaches (*e.g.,* Ref. [26]) where, with high statistics, the analysis can be performed with uncertainties as low as 5%; and

- Verify the duality assumption. At high statistics the measurement can be performed in large bins of M_x, thus checking the stability under the duality assumption.

Based on these arguments, while the current analysis has an error of about 14% in total (7% stat., 10% sys., 7% th.) it should be possible to approach asymptotically a total error of about 7% (5% sys and 5% theoretical).

6.4.2 Effect of detector improvements

Within the activity of the long term planning task force possible detector upgrades that could improve the measurement have been considered and are discussed in the following.

K^0_L identification. About 25% of the background in our analysis is originates from D decays into K^0_L mesons, which are then misidentified as photons. In order to have a significant impact on the sensitivity of the measurement a K^0_L selector with high efficiency is needed. Of course low photon contamination is also required in order to retain a high signal efficiency. No such selector is available currently, so the study has not been carried further although it might warrant additional work.

Low angle veto. Better hermeticity of the detector would help the measurement because it would improve the M_x resolution and reduce tails. However, for this purpose, we need to measure the energy of the particles in a larger solid angle. A simple veto on forward going particles is not useful: the background events that would be vetoed by such a detector would be events that already failed the requirement of the missing mass consistent with zero.

Vertex reconstruction improvement. The impact of the possible improvement of the performances of the SVT (see Section 3.3) has been studied. The $b \to c\ell\nu$ background differs from the signal because the hadronic decay products X come mostly from the decay of long living D mesons as opposed to the B meson or strong resonances. The distance between the vertex of the X system and the B decay vertex can therefore be used to discriminate between signal and background. Two vertices need to be determined:

- A vertex for the system X, obtained by finding the common vertex of the tracks involved; and

- A B decay vertex, obtained from the decay position of reconstructed B candidate and its line of flight, an inferred pseudo-track constructed to represent the recoiling B candidate and its intersection with the lepton trajectory [8].

Several quantities have been considered as possible discriminants:

- The distance between these two vertices in the xy plane (d_{xy}) or this quantity divided by its error (s_{xy}); and
- The distance between these two vertices in three dimensions (d_{3d}) or this quantity divided by its error (s_{3d}).

The distribution of these quantities on signal and background MC are shown in Fig. 20 and 21.

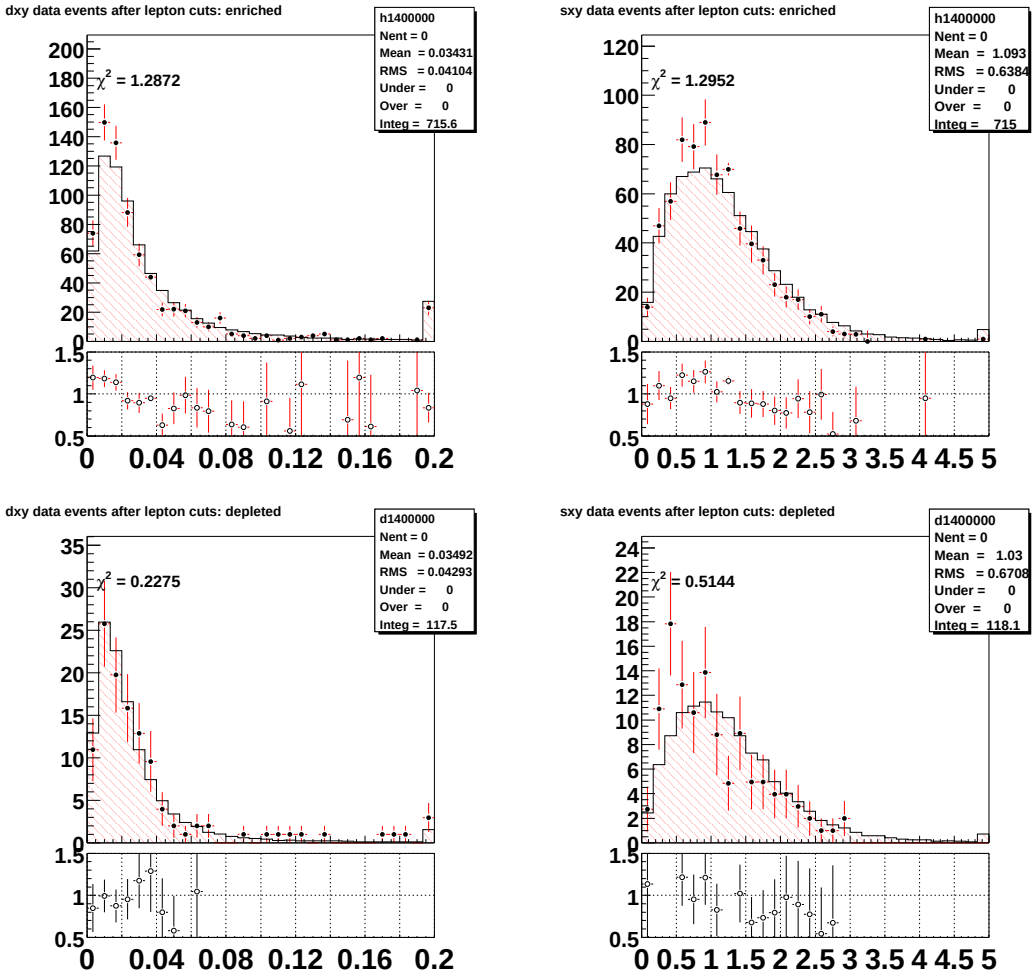

Figure 20: Distribution of a) d_{xy},b) s_{xy} for signal (dots) and background (histogram)

The resolution on the distance between the vertices is about $150\,\mu$m (as in the $\sin 2\beta$ analysis) and therefore comparable with the flight length we want to discriminate on. As expected, the distributions show that there is not enough separation power. In order to estimate the impact of improved SVT performance, the selected events are run through the Pravda simulation in a configuration that incorporates an additional silicon layer at 1.5 cm (Section 3.3). The distribution of d_{3d} and s_{3d} with the improved SVT is shown

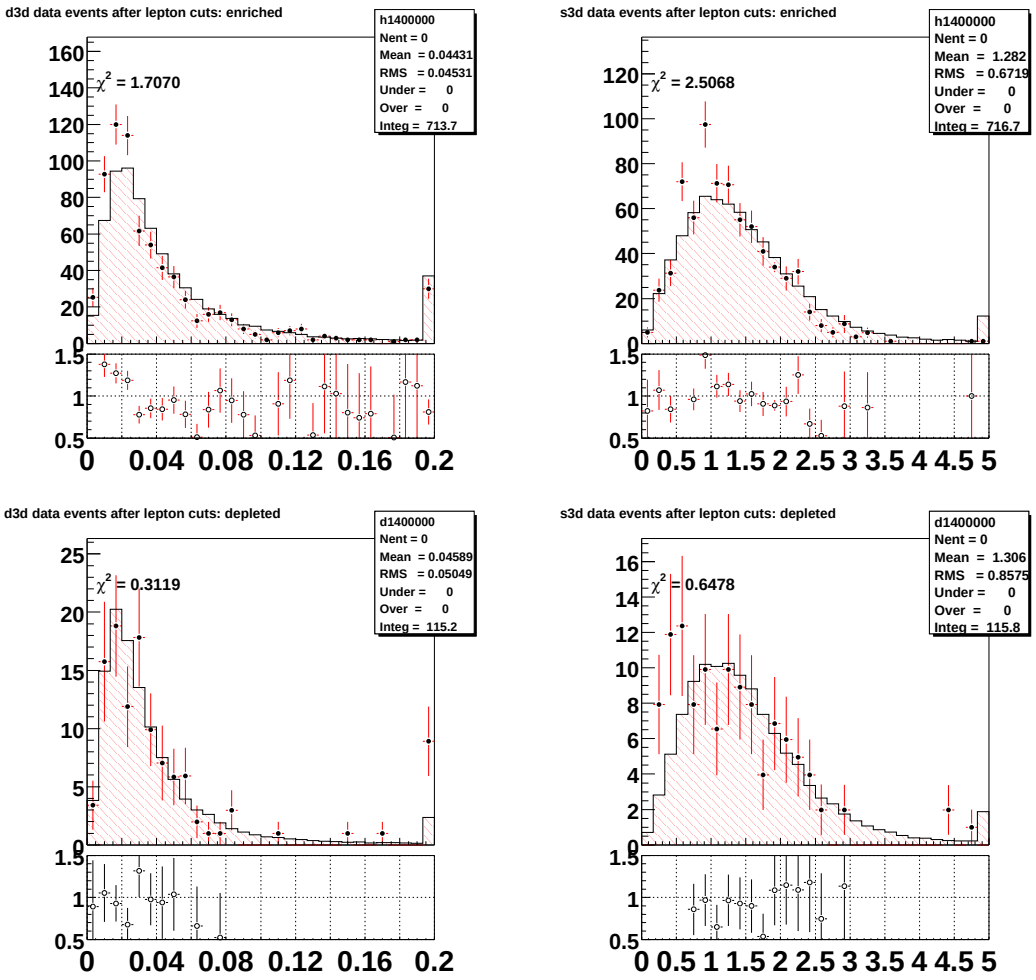

Figure 21: Distribution of a) d_{3d}, and b) s_{3d} for signal (dots) and background (histogram)

in Fig. 22. Table 21 quantifies the possible improvements in the measurement of V_{ub}, in terms of signal purity (which scales linearly with the systematic error) and statistical error. The absolute scale of the error is arbitrary (*i.e.,* depends on the simulated luminosity). Clearly, the improvement is quite marginal.

6.5 Extraction of V_{td} from $B \to \rho\gamma$

The effective flavor-changing neutral current processes $B \to \rho\gamma$ and $B \to \omega\gamma$ probe physics at high mass scales both within the Standard Model and within the context of possible new physics scenarios through the underlying $b \to d\gamma$ "penguin" transition [28]. The decays are analogous to the $B \to K^*\gamma$ process mediated by the $b \to s\gamma$ transition. The expected rate of $b \to d\gamma$ transitions is suppressed by the ratio of CKM matrix elements $|V_{td}/V_{ts}|^2$ relative to $b \to s\gamma$ transitions. There has been considerable interest recently in these exclusive channels, resulting in several calculations of the branching fractions

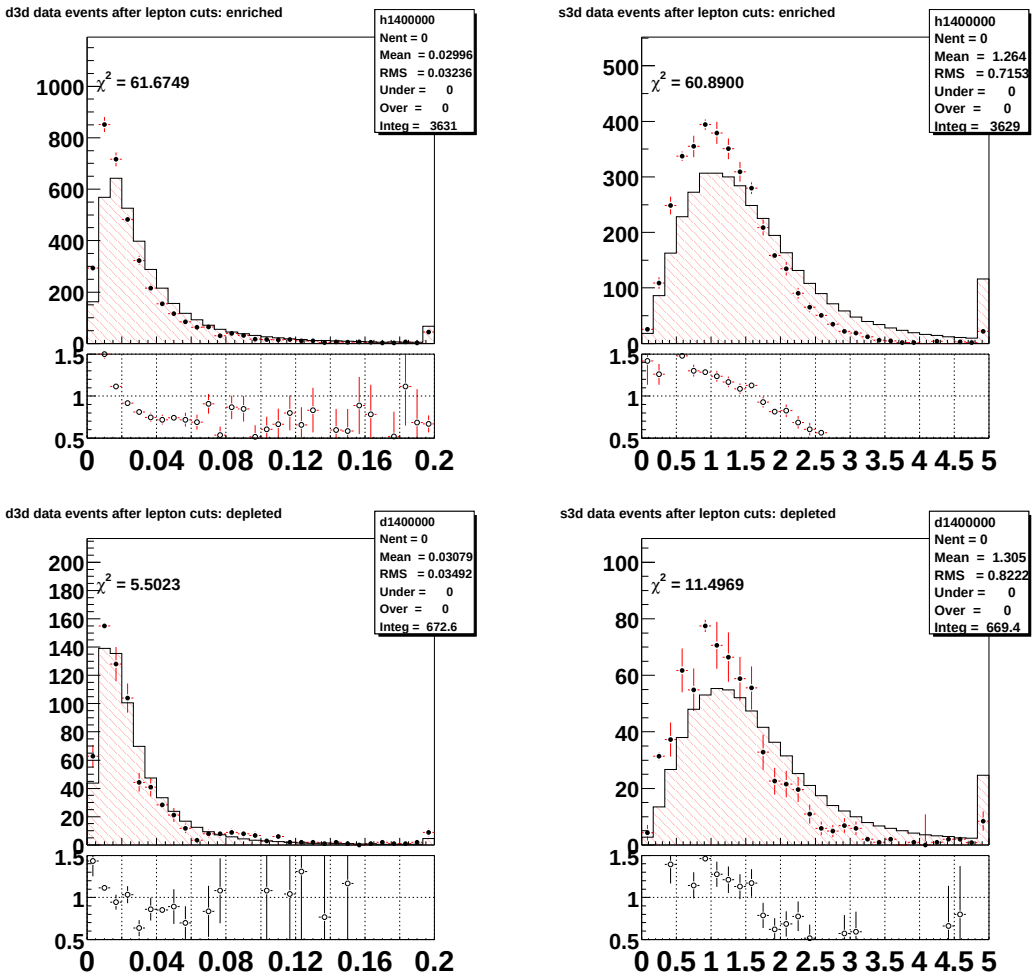

Figure 22: Distribution of a) d_{3d} and b) s_{3d} in signal (dots) and background (histogram) with the improved SVT configuration.

expected in the Standard Model, which indicate a range $\mathcal{B}[B^+ \to \rho^+\gamma] = (0.9-1.5)\times 10^{-6}$ [29]. Though the theoretical uncertainties for the branching fractions remain large, the possibility of extracting the ratio of CKM elements $|V_{td}/V_{ts}|^2$ through the ratio $\mathcal{B}[B \to (\rho/\omega)\gamma]/\mathcal{B}[B \to K^*\gamma]$ with less uncertainty has been explored [30] [31]. Ali *et al.* give the following expression for the ratio:

$$\frac{\mathcal{B}[B \to \rho\gamma]}{\mathcal{B}[B \to K^*\gamma]} = \left|\frac{V_{td}}{V_{ts}}\right|^2 \left(\frac{1 - m_\rho^2/M_B^2}{1 - m_{K^*}^2/M_B^2}\right)^3 \zeta^2[1 + \Delta R],$$

with $\zeta = 0.76 \pm 0.06$ and $\Delta R < 0.25$.

The observation of $B \to \rho\gamma$ and $B \to \omega\gamma$ would constitute the first evidence of the $b \to d\gamma$ radiative transition and is of considerable interest as the first step towards extracting $|V_{td}/V_{ts}|$ from measurements of these channels. Previous searches have found no evidence for these decays [32]. *BABAR* showed results based on 78 fb^{-1} at ICHEP [33]

	Relative error (%)	S/B	$\epsilon(V_{ub})(\%)$
Default	4.3	0.80	30
New SVT $S_{3d} < 2$	4.3	0.99	27
New SVT $S_{3d} < 3$	4.1	0.90	30

Table 21: Relative error on V_{ub}, signal over background and signal efficiency for several configuration, the default with no selection on the vertexing, the improved SVT with a cut on the 3-dimensional significance at 2 and with a cut at 3.

and quoted the following limits on the individual modes:

$$\mathcal{B}[B^0 \to \rho^0\gamma] < 1.4 \times 10^{-6}$$
$$\mathcal{B}[B^+ \to \rho^+\gamma] < 2.3 \times 10^{-6}$$
$$\mathcal{B}[B^0 \to \omega\gamma] < 1.2 \times 10^{-6}$$

The results can be combined into a single limit on the generic process $B \to \rho\gamma$ by assuming

$$\mathcal{B}[B \to \rho\gamma] = \mathcal{B}[B^+ \to \rho^+\gamma] = 2 \times \mathcal{B}[B^0 \to \rho^0\gamma] = 2 \times \mathcal{B}[B^0 \to \omega\gamma]$$

The limit obtained in this way was reported as

$$\mathcal{B}[B \to \rho\gamma] < 1.9 \times 10^{-6}.$$

6.5.1 Sensitivity extrapolations

We extrapolate the current analysis to higher luminosities with the following assumptions:

- The true branching ratios are given by:
  $\mathcal{B}[B^+ \to \rho^+\gamma] = 2 \times \mathcal{B}[B^0 \to \rho^0\gamma] = 2 \times \mathcal{B}[B^0 \to \omega\gamma] = 1 \times 10^{-6}$
- The statistical error on the branching ratio scales as $\mathcal{L}^{-1/2}$.
- The systematic error comes mostly from signal efficiency and so is "multiplicative". It has a statistical component that scales as $\mathcal{L}^{-1/2}$ and fixed component of 5%.
- The theory error on the ratio of $|V_{td}/V_{ts}|$ is 10%, which means that the theory error on $B \to \rho\gamma$ is 20%.

We also note that the analysis is currently dominated by continuum background. If this background could be reduced by a factor of two, then significantly improved sensitivity would result. In Fig. 23 we show plots of sensitivity extrapolations that are obtained using these assumptions.

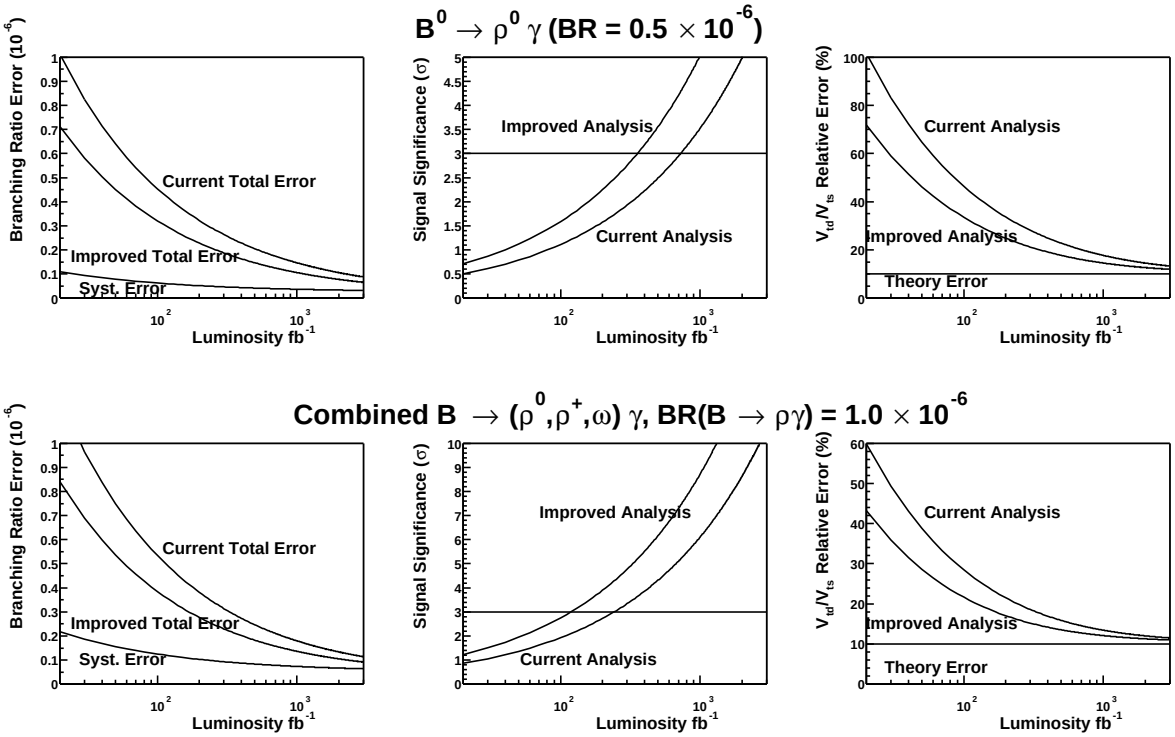

Figure 23: Sensitivity projections for $B \to \rho\gamma$ modes. The top row is for the mode $B^0 \to \rho^0\gamma$ and the bottom row is for $B^0 \to \rho^0\gamma$, $B^+ \to \rho^+\gamma$ and $B^0 \to \omega\gamma$ combined. In each plot, "Current" refers to the current analysis and "Improved" assumes that the continuum background rejection can be reduced by a factor of two. In each column, the left plot shows the total and systematic error as a function of luminosity; the center plot shows the expected signal significance; the right plot shows extracted error on V_{td}/V_{ts}.

6.5.2 Effect of detector improvements (photon veto)

It is apparent that an extra factor of two in continuum background rejection could make a large difference in the sensitivity of this analysis. In particular, it would give us an expected 3σ effect for the combined modes with roughly $100 fb^{-1}$. Therefore, it is worth thinking about where this extra background rejection might come from.

The largest source of background high-energy photons is $\pi^0 \to \gamma\gamma$ and $\eta \to \gamma\gamma$. These events can be rejected by finding the "sister" photon of the high-energy photon that is being used in the B candidate. We will call the high-energy photon from this decay the "candidate" photon. There are three requirements that are used to veto the "sister" photon in these decays:

- Photon isolation requirement: no neutral bumps with $E > 50\,\mathrm{MeV}$ within 25 cm of the candidate photon;
- π^0 veto: $E_\gamma > 50\,\mathrm{MeV}$ and $|m_{\gamma\gamma} - m_\pi^0| < 20\,\mathrm{MeV}/c^2$, where E_γ is the energy of any neutral bump in the event and $m_{\gamma\gamma}$ is the mass of that bump and the candidate

photon; and

- η veto: $E_\gamma > 250\,\mathrm{MeV}$ and $|m_{\gamma\gamma} - m_\eta^0| < 40\,\mathrm{MeV}/c^2$.

The E_γ requirements are needed so that "junk" photons are not allowed to artificially reject events and the $\mathrm{m}_{\gamma\gamma}$ requirements represent roughly 3σ intervals. The selection requirements were optimized for the $B \to K^*\gamma$ analysis and might end up in very slightly different positions for $B \to \rho\gamma$ analysis. However, since the $m_{\gamma\gamma}$ requirement is already very loose, loosening it further is unlikely to give much more rejection.

A more fruitful approach might be to find what's happening to the "missing" photons. If, for example, they are all escaping out the forward or backward holes in the EMC, then this might be fixed by a simple veto counter. In order to study this question, we used a sample *uds* Monte Carlo and ran our usual $B^0 \to \rho^0\gamma$ reconstruction. We then recorded the Monte Carlo truth information of the "sister" photons. and examined the effect of the above photon veto requirements on these photons. Since we are looking at the truth information, there is no requirement that the sister photon was reconstructed, or even that it is in the active region of the detector. Figure 24(a) shows the polar angle distribution for these sister photons before and (b) after the photon veto requirements are applied. One can see that photons in the very forward ($\cos\theta > 0.95$) and ($\cos\theta < -0.8$) are not vetoed efficiently because they go into the "holes" of the EMC.

Figure 24(c) shows the efficiency of the photon veto requirements and indicates that for photons in the central region of $\cos\theta$, the inefficiency of the vetoes is about 10%. In the far forward and background regions, this inefficiency goes up considerably, as expected. However, as shown in 24(b), the fraction of photons in these regions is rather small, comprising only a few percent of the total, even after the photon veto requirements have been applied.

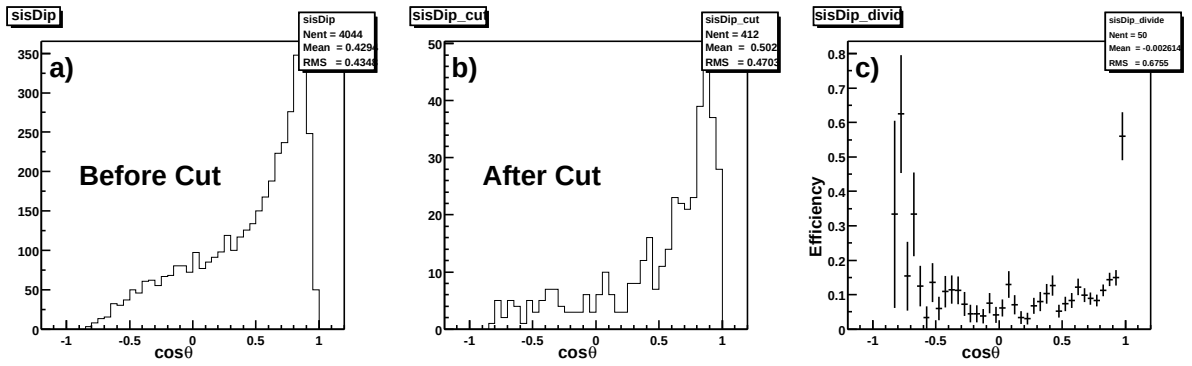

Figure 24: Distributions of the Monte Carlo truth value of the cosine of the polar angle for sister photons of candidate photons coming from π^0's, a) before any photon veto requirements have been applied, b) after the photon veto has been applied, and c) the ratio of b) and a) - the efficiency of the photon veto requirements for rejecting background.

This means that filling these holes in the forward and backward regions would have little effect on the overall veto inefficiency. Rather, we need to understand the what is

happening to the "missing" photons in the central region. A large fraction of these (about 40%) are simply below the E_γ threshold of 50 MeV. This threshold is difficult to lower because of the large number of "junk" photons below this cutoff. Understanding how the photons with $E_\gamma > 50$ MeV are lost is a subject of ongoing work.

6.6 Searches for $B^- \to \tau^- \overline{\nu}_\tau$ and $K^- \nu\overline{\nu}$

$B^- \to \tau^- \overline{\nu}_\tau$ and $B^- \to K^- \nu\overline{\nu}$ are exclusive rare B decay modes with SM branching fractions predicted to be at the level of $\sim 5 \times 10^{-5}$ and $(3-5) \times 10^{-6}$ respectively. Neither mode has yet been observed. These modes are difficult experimentally due to the the presence of two or more neutrinos in the final state, resulting in significant missing energy and very limited kinematic information which can be exploited to identify the signal mode. *BABAR* currently has preliminary branching fraction limits of $\mathcal{B}(B^- \to \tau^- \overline{\nu}_\tau) < 4.1 \times 10^{-4}$ [34]. and $\mathcal{B}(B^- \to K^- \nu\overline{\nu}) < 7.0 \times 10^{-5}$ [35]. Since the two modes possess similar experimental signatures, they will be discussed together here.

The signature for $B^- \to \tau^- \overline{\nu}_\tau$ and $B^- \to K^- \nu\overline{\nu}$ is a charged B meson decaying to a single charged particle (e, μ,π or K) and few or no additional neutral particles[2]. In practice, in B mesons produced at the $\Upsilon(4S)$ it is not possible to distinguish particles associated with the decay of the "signal" B^- with those of the "companion" B^+ using only the kinematics of the signal B^-. Consequently, the analysis proceeds by first cleanly identifying the decay products of the companion B^+ by fully reconstructing it in known hadronic or semileptonic decay modes, and then searching for the expected low-multiplicity–plus–missing-energy signature in the tracks and clusters remaining after those associated with the companion B^+ reconstruction have been removed.

This method has a number of pertinent features, which effect extrapolation to high-luminosity scenarios:

- The overall signal selection efficiency is dominated by the rather low *companion* B^+ reconstruction efficiency, rather than the signal B^- efficiency;
- The fact that the signal B^- has low multiplicity results in a higher purity of the companion B^+ reconstruction than would be found for "generic" B^- decays. This permits the use of B^+ reconstruction modes which would be to "dirty" for use in other contexts; and
- The companion B^+ reconstruction strongly suppresses $B^0\overline{B}^0$ and continuum events compared to B^+B^- events. This dictates that the dominant backgrounds will be due to other B^- decays faking the signal mode signature provided the companion B^+ selection is sufficiently clean. If continuum backgrounds are found to contribute significantly, the selection can be simply be tightened so as to reject it.

Two methods are currently being used for the companion ("tag") B^+ reconstruction and are discussed here. The first is the *semi-exclusive* hadronic B reconstruction [25], which selects candidates of the type $B^+ \to D^{(*)0}\{l\pi^\pm + nK^\pm + m\pi^0\}$ and the D^0 is exclusively reconstructed to the modes $K\pi$, $K\pi\pi^0$, $K\pi\pi\pi$ and $K^0_s\pi^+\pi^-$. The second

[2]The τ^- can of course also decay via higher multiplicity modes but these are not considered here.

method is a $B \to D\ell\nu X$ reconstruction [35], in which an exclusively reconstructed D^0 is combined with a hard lepton, and the additional daughters "X" are either nothing or photons consistent with feeddown from higher-mass charm states (D^{*0}, D^{**0} etc.). The first method has a cleaner reconstruction and consequently the potential to have lower continuum and mis-reconstruction background rates, while the second has a somewhat higher reconstruction efficiency.

Sample	Efficiency		Theory	Yield			
	Signal	Reco $[\times 10^{-3}]$	prediction	$0.1\,\mathrm{ab}^{-1}$	$0.5\,\mathrm{ab}^{-1}$	$2\,\mathrm{ab}^{-1}$	$10\,\mathrm{ab}^{-1}$
$B^- \to \tau^- \overline{\nu}_\tau$	0.2	1–1.5	5×10^{-5}	~ 1	6	24	120
	0.2	5		6	36	144	720
$B^- \to K^- \nu\overline{\nu}$	0.3	1–1.5	4×10^{-6}	0.1	0.7	3	13
	0.2	5		0.4	2	9	44

Table 22: Expected yields for $B^- \to \tau^- \overline{\nu}_\tau$ and $B^- \to K^- \nu\overline{\nu}$ and the associated "tag" B^+ reconstruction.

The signal B^- selection requires that there is only a single track not associated with the tag B^+, that the track satisfy the appropriate (tight or very tight) PID for $B^- \to \tau^- \overline{\nu}_\tau$ (e, μ, π) or $B^- \to K^- \nu\overline{\nu}$ (K) and that there is a total of less than 300 MeV of energy in additional clusters (GoodPhotonLoose). Events with good π^0 or K^0_S candidates are also explicitly vetoed. The signal and tag efficiencies and expected yields are given in Table 22.

As previously noted, relevant backgrounds are predominantly from B^+B^- events in which the B^+ is correctly reconstructed and the B^- has low observed track and cluster multiplicity in the detector. Such events are caused by a failure to reconstruct observable particles (*i.e.,* particle passing outside of the detector acceptance or falling below kinematic thresholds for tracking or calorimetry), by the presence of neutrinos or unreconstructed neutral hadrons (K^0_L), or a combination of both. Since these backgrounds do not involve cross-feed between the signal and tag B, the background rates should be comparable with either tag sample. Estimates of the expected level of irreducible backgrounds were therefore obtained using samples of hadronic "BReco cocktail" MC samples in which one B decays generically and the second decays to modes which have high reconstruction efficiency for the SemiExclusive tag.

Assuming a perfect detector (*i.e.,* using MC truth), topologically irreducible backgrounds to both $B^- \to \tau^- \overline{\nu}_\tau$ and $B^- \to K^- \nu\overline{\nu}$ appear to be at or below the SM rates for these modes, although this does not take into account either the geometrical acceptance or kinematic thresholds for tracking and calorimetry. Applying a more realistic event selection in SP4 MC with the present detector configuration yields B^+B^- backgrounds at the levels of approximately 8×10^{-4} and 2×10^{-5} respectively, so it is clear that in the absence of additional rejection power S/B is expected to be somewhat less than one for both of these modes.

In both $B^- \to \tau^- \overline{\nu}_\tau$ and $B^- \to K^- \nu\overline{\nu}$, more than half of these backgrounds are attributable to B^- events containing one or more K^0_L. Note that the constraints on the

EMC cluster multiplicity and energy already suppress events with a K_L^0 which interacts in the EMC, so the remaining K_L^0 backgrounds are due to IFR-only or "undetectable" K_L^0's. At present, the performance of the IFR is inadequate to permit the use of an meaningful veto on IFR-only K_L^0's.

The lower background rate for $B^- \to K^-\nu\overline{\nu}$ is due to three factors: the requirement of a charged kaon suppresses pion backgrounds; the hard momentum spectrum of the signal kaon permits a momentum cut of $p_{CM} > 1.5\,\mathrm{GeV}/c$; the presence of a charged kaon makes it less likely that there will be K_L^0 (*i.e.,* a second s quark) in the event.

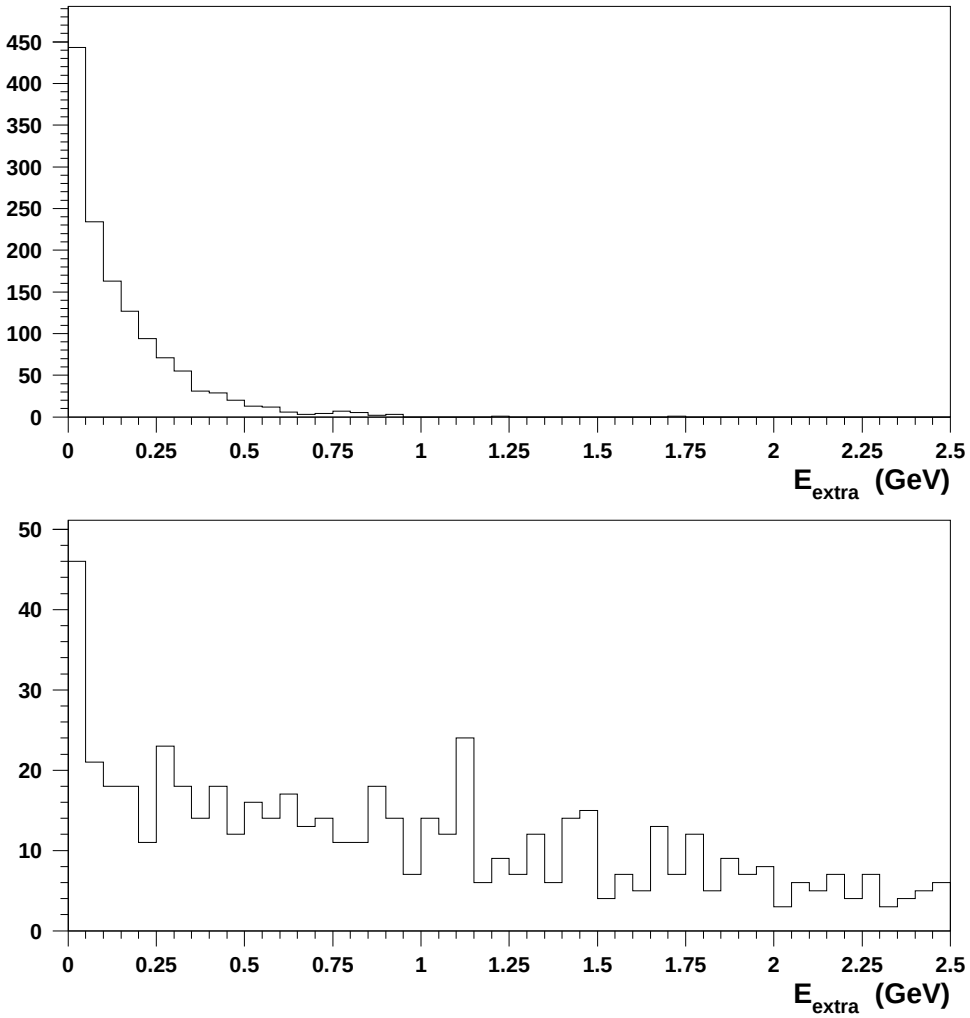

Figure 25: Distribution of the total energy, E_{extra}, of remaining EMC clusters after removing those associated with the reconstructed B^+ and the $B^- \to K^-\nu\overline{\nu}$ candidate decay, for (top) $B^- \to K^-\nu\overline{\nu}$ signal MC and (bottom) generically decaying B^- MC.

Some additional rejection power can likely be obtained beyond the quoted limits by optimization of the selection algorithm, but it is unlikely that the improvement would be dramatic. Because of the relatively low S/B ratio, the $B^- \to \tau^-\overline{\nu}_\tau$ or $B^- \to K^-\nu\overline{\nu}$ signal would have to be obtained from a small excess of events above a background,

most likely using a fit to the candidate signal track momentum spectrum. In the case of $B^- \to \tau^- \overline{\nu}_\tau$, a simultaneous fit to several τ decay modes would be used, with the relative yields constrained by the measured branching fractions. Since the dominant backgrounds are from B decay modes with low and poorly known branching fractions and containing neutral hadrons which are not well modeled in the present simulation, it is likely that the $B^- \to \tau^- \overline{\nu}_\tau$ or $B^- \to K^- \nu \overline{\nu}$ determinations will be limited by detector-related systematics.

Improvement of the detector angular acceptance would permit the recovery of some portion of the particles lost in the forward direction, resulting in a larger average measured multiplicity in B^+B^-, and so presumably a lower rate of background events faking the signal mode topology.

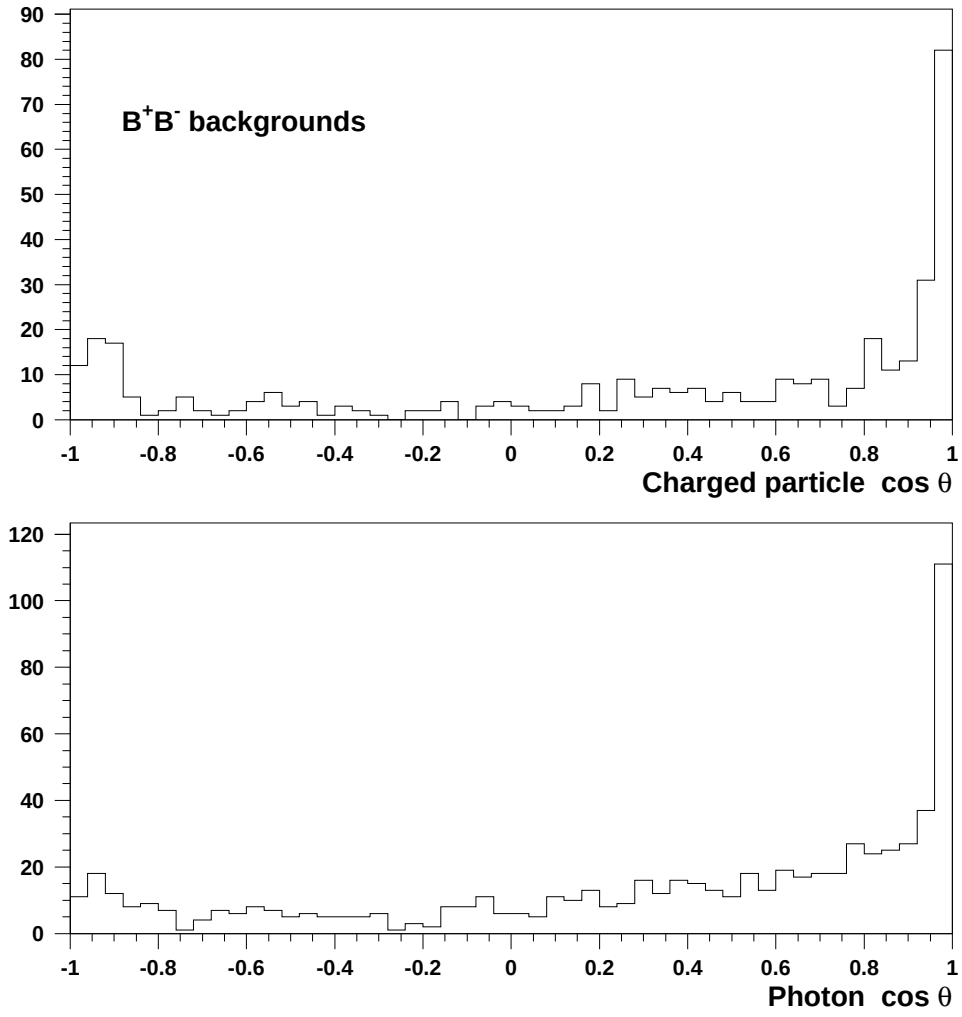

Figure 26: Angular distribution of charged (top) and neutral (bottom) particles from B^- decays, obtained from MC truth for generic B^+B^- events, which pass the full $B^- \to \tau^- \overline{\nu_\tau}$ selection. Peaks in the forward and backward direction indicate a contribution from events with undetected particles outside the current detector acceptance.

The total measured EMC energy, E_{extra}, of neutral clusters which are not associated with the reconstructed B^+ or the expected $B^- \to \tau^- \overline{\nu}_\tau$ or $B^- \to K^- \nu\overline{\nu}$ signal candidate are shown in Fig. 25. For a perfect detector and reconstruction algorithm, this quantity should be zero for signal events. However mis-reconstruction, contributions from hadronic split-offs, beam backgrounds, etc., significantly broaden it for real events. A typical analysis cut is $E_{extra} < 300\,\mathrm{MeV}$. Loss of particles outside of the acceptance causes background events to shift towards low values of E_{extra}, *i.e.,* into the signal region.

Figure 26 shows the θ distribution for charged and neutral particles (from MC truth) in simulated B^+B^- background events that have passed the full $B^- \to \tau^- \overline{\nu}_\tau$ event selection, indicating that a significant fraction of background events have missing particles. In practice, very few B^+B^- events lose sufficient energy in this manner to fake a signal event topology without additional contributions from missing neutrinos or neutral hadrons.

In a scenario in which the region from $200-300$ mr is assumed to be instrumented with a "veto" device (*i.e.,* no forward tracking, and no usable energy resolution), it appears that only about a 10% reduction in overall backgrounds rates would be obtained. Note that this does not take into account the probable high rate of beam backgrounds in such a device, which would further degrade its utility for this analysis. Given the expectation of a relatively high S/B and the fact that the present angular acceptance is comparatively well modeled in MC, this reduction is not likely to result in a significant improvement in the sensitivity for $B^- \to \tau^- \overline{\nu}_\tau$ or $B^- \to K^- \nu\overline{\nu}$.

7 Conclusions and recommendations

PEP-II and *BABAR* have been remarkably successful in reaching, within 3 years of initial collisions, the point where *CP* violation has not only been demonstrated in B^0 decays, but has even become a precision measurement. While measurements of $\sin 2\beta$ are in good agreement with the predictions of indirect constraints for CKM matrix elements, there is still a rich program of exploring the full range of *CP* violation effects in B decays. Access to *CP* violation in many channels, the ability to search for new physics in rare decays, and the need to improve the precision of our determinations of CKM matrix elements remain the strengths of the B Factory experiments. PEP-II is already in the process of implementing a program of luminosity upgrades that should lead to an integrated $0.5\,\mathrm{ab}^{-1}$ by the end of 2006. The long-range task force has identified additional steps at PEP-II or *BABAR*, which may lead to further improvement in the physics reach of the experiment. Having quantified the physics impact of these upgrades, we have drawn the following conclusions.

Implementation of Small-Angle Crossing Scheme. Many important *CP* and rare decay physics analyses will remain statistically limited with a $0.5\,\mathrm{ab}^{-1}$ data sample that is the goal for PEP-II and *BABAR* by the end of 2006. For example, comparisons of $\sin 2\beta$ from modes other than $b \to c\overline{c}s$ will not reach an interesting level of sensitivity. Unraveling the penguin contribution to $\sin 2\alpha_{eff}$ will not be possible. Extraction of γ from $B^\pm \to D^0 K^\pm$ will probably not yield interesting results due to a combination of large

errors and overlapping ambiguities. Each of these analyses would benefit significantly from a much larger data sample.

Staying within the physical limits of the LER vacuum system, an additional factor of two improvement in PEP-II peak luminosity appears to be attainable. This project would entail modest changes to the IR configuration to allow for more focusing of the LEB while retaining good beam separation at parasitic crossing by introducing a small-angle crossing scheme. Two additional rf stations would also be required. The total cost of this investment is estimated to be \$12–14 million.

These changes, if implemented in coordination with the planned horizontal module replacement for the SVT, would probably have a minimal impact on the total down time for PEP-II and *BABAR*. The present schedule calls for module replacement in the summer of 2005. This would impose a rather tight schedule on the design and fabrication of replacement B1 magnets. However, we anticipate some degree of flexibility on the exact timing of this intervention. It should be noted that a major portion of the barrel RPC replacement will also occur in the 2005 down period.

If implemented in 2005, so that the full benefit of the luminosity improvement might be seen by the end of 2006 ($0.4\,\mathrm{ab}^{-1}$/year for 2007–2009), it is conceivable that this schedule would lead to a total integrated sample of 1.5–$2\,\mathrm{ab}^{-1}$ by the end of 2009. While it is possible that LHCb and perhaps BTeV will be operational by then, we believe that there will continue to be many unique capabilities of the B factory experiments that can be exploited in a complementary fashion. Plans for luminosity improvements at KEKB remain somewhat uncertain beyond the design value of 1×10^{34} $\mathrm{cm}^{-2}\mathrm{s}^{-1}$. However, we assume that this will remain a tight competition as well throughout the decade.

Recommendation 1. SLAC should proceed with funding required to develop the modified IR for small-angle crossing as soon as possible. The installation of the replacement IR components should be coordinated with the SVT horizontal module replacement.

Modifications to SVT. No compelling physics benefit has been identified for the reduction of the beam pipe and addition of another layer (L_0) to the SVT. The feasibility for implementing such a project is also not established. Our assessment is that the cooling and SR masking problems associated with a reduced radius would be difficult to solve, and would likely lead to orbit restrictions that could be inconsistent with high operational efficiency.

Recommendation 2. The SVT should be retained in its present configuration, with midplane module replacement as required by radiation consideration, but likely in 2005.

B1 instrumentation. It appears that the technical risks associated with instrumenting B1 as a veto detector are small. This would be a small-scale and relatively inexpensive project to implement. However, the technical feasibility, in particular the background rates, is not yet established. In addition, the physics benefit of such instrumentation appears to be quite small. New backgrounds instrumentation has been added around

the present B1 magnets in the summer of 2002. This should allow for a quantitative assessment of the feasibility of the project.

Recommendation 3. The Technical Board should re-examine the feasibility of instrumenting B1, based on information obtained from the new background detectors. If it appears viable and a a real physics case can be established, then proceeding with this project may be sensible.

Backgrounds. Several systems appear to be vulnerable to background problems at the highest luminosities. However, we note two important caveats to this statement. First, the design of the small crossing-angle IR was not advanced enough to allow a renewed look at changes to projected background conditions that might result. Second, many or the detailed studies that are the basis for the extrapolations date from some time ago, from a time when the PEP-II/*BABAR* backgrounds group was still active.

The SVT horizontal modules are estimated to have a 2-year lifetime in terms of integrated radiation dosage. Clearly it is not feasible to expect a biannual replacement program, both from the standpoint of effort to build modules and the down time needed to replace them.

The DCH occupancy in the inner superlayer may not be tolerable, although this point was unclear to us from existing studies. Further work should be done to understand this problem and determine whether it will indeed be a concern at the highest luminosities.

The forward and rear IFR endcaps will likely have background problems around the beam line, in addition to those already evident in the outermost layers. The barrel should not represent a problem in this regard.

Recommendation 4. *BABAR* and PEP-II should revive a machine-detector backgrounds group, both to provide continuing improvement of instrumentation and background conditions, and as the basis for optimization of backgrounds in a re-design of the IR.

Recommendation 5. The SVT, DCH, and IFR systems should commission detailed studies of anticipated backgrounds at 4×10^{34} cm^{-2}s^{-1} and devise a long-term plan to preserve the performance of these detector systems through 2010.

DAQ limitations to to DCH readout. It appears that the DAQ system for the DCH will limit the L1 trigger rate to about 4 kHz. Based on present projections of the trigger rates, deadtimes will be in the range 3–8% at 2×10^{34} cm^{-2}s^{-1} and 15-30% at 4×10^{34} cm^{-2}s^{-1} if nothing is done to trigger or DCH readout. The options available are

Option I: Remove the DCH bottleneck by rearranging dataflow downstream of the FEA boxes to use additional optical fibers. This option has implications for offline storage and computing that should also be considered; and

Option II: Tighten the L1 trigger to maintain a L1 rate below 4 kHz.

Recommendation 6. Since the lead time in dealing with this problem is about 1 year, the question of which strategy to adopt should be revisited by the Technical Board at the end of the 2003 run, in order to obtain better projections of the background and trigger rates. The decision should also recognize the wider implications of recording large amounts of data that are not used for physics.

A Charge to task force on long-term upgrades

A Task Force on Long-Term Upgrades is being formed to advise *BABAR* management on the optimal feasible upgrade path, which maximizes the physics reach of the experiment on a mid-to-long term time scale. The specific goal is to understand the best possible strategy for maintaining leadership of *BABAR* in heavy flavor physics over the medium term period starting in 2006 and extending for an additional 4–5 years. However, it should also consider these upgrades in the context of nascent proposals for collider designs that aim at 10^{36} cm^{-2}s^{-1} luminosities.

It is intended that the Task Force work in close cooperation with the Technical Board and the PAC/AWG team. In particular, it is expected the Task Force will need to commission specific studies including, but not limited to, background projections, technical feasibility, conceptual engineering, analysis projections and Monte Carlo simulation of existing or modified detector performance. These studies will be specifically targeted to allow a reasonable assessment of upgrade options, but will rely on the support of the Technical Board and PAC/AWG team.

The Task Force is formed of 2 groups: Group 1 (Physics) and Group 2 (Detector). Group 1 and Group 2, are considered two parts of the same Task Force, and therefore should interact closely and work in a coherent way. The coordinators of the two groups are specifically asked to place an emphasis on maintaining such a close interaction between the two groups, the Technical Board, and the PAC/AWG team.

A.1 Charge to Group 1

Establish a limited set of benchmark physics processes, chosen on the basis of their physics impact, as well as their sensitivity to the performance of complementary aspects of the present or upgraded detector. Study and evaluate the limitations of the present or upgraded detector, due to luminosity, tracking and vertex resolution, missing energy/momentum determination, high-energy π^0 and γ reconstruction, and PID separation, where applicable. A possible set of benchmark analyses would include, but is not limited to, the following or their equivalent:

- Precision determination of sin2β, as it approaches a statistical error is 0.03 for example, and sensitivity to the difference in phases between various channels, such as ϕK^0_S versus $J/\psi\, K^0_S$;
- Extraction of α by means of the channels $B \to \pi\pi$, $\pi^0\pi^0$, $\rho\pi$;
- Extraction of f_B from $B \to \tau\nu$; and
- Search for rare decays that are sensitive to new physics (e.g., lepton flavor violation), such as $\tau \to \mu(e)\gamma$.

These benchmarks provide a means of evaluating various performance improvements under consideration and should be used to establish the physics reach of the experiment as a function of luminosity, both in the present configuration and after possible upgrades as suggested by Group 2.

A.2 Charge to Group 2

Working in close contact with PEP II and Group 1, establish a plausible set of input parameters for:

- Luminosity;
- Detector limits to physics performance as suggested by Group 1;
- Angular acceptance in the forward direction; and
- Machine background conditions

assuming a major, but still feasible upgrade of PEP-II and the interaction region on a timescale of 3–4 years from now. Evaluate the maximum possible improvement that can be obtained with minimal intervention to the detector, using as a measure:

- Statistical precision;
- Tracking/vertexing resolution;
- π^0 and γ reconstruction (in particular for high energy π^0's);
- PID separation;
- Missing energy/momentum determination ($B \to \tau\nu$ $B \to K\nu\overline{\nu}$; and
- Signal/background improvement in channels with many particles.

The improvements must balance cost, resources (including both facilities and manpower), time required, and the loss of beam time and integrated luminosity due to necessary installation, commissioning, or related tasks.

References

[1] Find PravdaMC reference

[2] W. Innes, "Trackerr: A Program for Calculating Tracking Errors", *BABAR* Note # 121 (1993).

[3] `f2c` can be downloaded at `http://netlib.org/f2c/`

[4] P. Billoir, Nucl. Instr. Meth. A **225**, 352 (1984).

[5] G.Lynch *et al.*, "*BABAR* Drift Chamber Tracking Conventions", *BABAR* Note # 488 (1999)..

[6] *BABAR*Collaboration, B. Aubert, *et al.*, Nucl. Instr. Meth. A **479**, 1 (2002).

[7] J. Beringer, "Analysis of B Flavor Tagging Performance and Study of Improvements from a Topological Tagging Algorithm", *BABAR* Analysis Document, # 502 (Sep 2002).

[8] *BABAR* Collaboration, B. Aubert, *et al.,* Phys. Rev. Lett. **87**, 091801 (2002).

[9] *BABAR*Collaboration, B. Aubert em et al., "Measurement of time-dependent *CP* asymmetries and the *CP*-odd fraction in the decay $B^0 \to D^{*+}D^{*-}$", *BABAR* Analysis Document # 548 (June 2003).

[10] *BABAR*Collaboration, B. Aubert em et al., "Study of time-dependent *CP* asymmetry in neutral B decays to J/ψ
piz", *BABAR* Analysis Document # 500 (May 2003).

[11] *BABAR*Collaboration, B. Aubert em et al., "Measurements of *CP* asymmetries and branching fractions in $B \to \phi K$ and $B \to \phi\pi$", *BABAR* Analysis Document # 541 (May 2003).

[12] *BABAR*Collaboration, B. Aubert em et al., "Measurements of *CP*-violating asymmetries and branching fractions in B meson decays to $\eta' K$", *BABAR* Analysis Document # 560 (March 2003).

[13] M. Gronau and D. London, Phys. Rev. Lett. **65**, 3381 (1990).

[14] *BABAR* Collaboration, B. Aubert, *et al.*, "Measurements of Branching Fractions and Direct *CP* Asymmetries in $\pi^+\pi^0$, $K^+\pi^0$ and $K^0\pi^0$ B Decays", contributed to the ICHEP 2002, hep-ex/0207065.

[15] *BABAR* Collaboration, B. Aubert, *et al.*, Phys. Rev. Lett. **89**, 281802 (2002).

[16] A. Roodman, http://www.slac.stanford.edu/h̃itlin/SuperBABAR/presentations/020122/pizpiz-22jan02.ps

[17] Y. Grossman and H. Quinn, Phys. Rev. D **58**, 017504 (1998).

[18] J. Charles, Phys. Rev. D **59**, 054007 (1999)

[19] A. Ali, *et al.*, Phys. Rev. D **58**, 094009 (1998); C. Isola, *et al.*, Phys. Rev. D **65**, 094005 (2002); Y. F .Zhou, *et al.*, hep-ph/0006225; Also see [18]

[20] A. Bevan, "A long term planning study on using the Grossman-Quinn bound", *BABAR*Analysis Document # 504 (2002).

[21] M. Gronau and D. Wyler, Phys. Lett. B **265**, 172 (1991); M. Gronau and D. London, Phys. Lett. B **253**, 483 (1991).

[22] G. Batignani, *et al.*, "Analysis of $B^- \to D^0_{(CP)}K^-$ decays", *BABAR* Analysis Document # 404, (2002).

[23] *BABAR* Collaboration, B. Aubert, *et al.*, "A study of $B^- \to D^0_{(CP)}K^-$ decays", contributed to the ICHEP 2002, hep-ex/0207087.

[24] C. Bozzi, *et al.*, "Measurement of the Inclusive Charmless Semileptonic Branching Ratio and the Determination of $|V_{ub}|$", *BABAR* Analysis Document # 347 (2002).

[25] D. del Re *et al.*, "Semi-Exclusive B Reconstruction", *BABAR* Analysis Document # 271 (2001).

[26] U. Aglietti, M. Ciuchini, P. Gambino, Nucl. Phys. B **637**, 427 (2002).

[27] *BABAR* Collaboration, B. Aubert, *et al.,* Phys. Rev. D **66**, 032003 (2002).

[28] See for example, S. Bertolini, F. Borzumati and A. Masiero, Nucl. Phys. B **294**, 321 (1987); H. Baer, M. Brhlik, Phys. Rev. D **55**, 3201 (1997); J. Hewett and J. Wells, Phys. Rev. D **55**, 5549 (1997); M. Carena *et al.*, Phys. Lett. B **499**, 141 (2001).

[29] M. Beneke, T. Feldmann and D. Seidel, Nucl. Phys. B **612**, 25 (2001); S. W. Bosch and G. Buchalla, Nucl. Phys. B **621**, 459 (2002).

[30] A. Ali and A. Y. Parkhomenko, Eur. Phys. Jour. C **23**, 89 (2002).

[31] B. Grinstein and D. Pirjol, Phys. Rev. D **62**, 093002 (2000).

[32] CLEO Collaboration, T.E. Coan *et al.*, Phys. Rev. Lett. **84**, 5283 (2000); Belle Collaboration, Y. Ushiroda *et al.*, contributed to BCP4, Ago Town, Japan, Feb 2001, hep-ex/0104045.

[33] *BABAR* Collaboration, B. Aubert, *et al.,* "Search for the Exclusive Radiative Decays, $B \to \rho\gamma$ and $B^0 \to \omega\gamma$", contributed to the ICHEP 2002, hep-ex/0207073.

[34] *BABAR* Collaboration, B. Aubert, *et al.*, "A Search for the Decay $B^+ \to \tau^+\nu_\tau$ Recoiling Against $B^- \to D^0\ell^-\overline{\nu}_\ell X$", contributed to Moriond 2003, hep-ex/0303034.

[35] *BABAR* Collaboration, B. Aubert, *et al.*, "A Search for the Decay $B^- \to K^-\nu\overline{\nu}$", contributed to Moriond 2003, hep-ex/0303xxx.